An overview of the Oden Arctic Technology Research Cruise 2015 (OATRC2015) and numerical simulations performed with SAMS driven by data collected during the cruise

Raed Lubbad [1] Sveinung Løset Wenjun Lu Andrei Tsarau Marnix van den Berg

(To be submitted to <Cold Regions Science & Technology> special issue)

Sustainable Arctic Marine and Coastal Technology (SAMCoT), Centre for Research-based Innovation (CRI)

Norwegian University of Science and Technology (NTNU), Trondheim, Norway

[1] Corresponding author
E-mail address: raed.lubbad@ntnu.no

Contents

Abstract

In the autumn of 2015, the Norwegian University of Science and Technology (NTNU) and the Swedish Polar Research Secretariat (SPRS) performed a research cruise named the "Oden Arctic Technology Research Cruise 2015" (OATRC2015); it involved the two Swedish icebreakers, Oden and Frej, in the international waters north of Svalbard. The ExxonMobil Upstream Research Company supported and participated in OATRC2015. The overall objective of OATRC2015 was to perform a safe cruise, collect valuable and important scientific data, and conduct full-scale field trials to test key technologies. The scientific scope of OATRC2015 included three major fields of study, namely: 1) collection of full-scale data necessary to build, calibrate and validate numerical models for floaters in ice, 2) collection of full-scale data necessary to build, calibrate and validate numerical models for ice management operations, and 3) collection of data for health, safety and environmental research. This paper presents OATRC2015, including the objectives of the expedition, and provides an overview of the research performed and the major findings. In addition, the paper includes an extensive discussion on the use of full-scale data from OATRC2015 to validate the Simulator for Arctic Marine Structures (SAMS).

Keywords:

OATRC2015, Full-scale data, Ice Management, Validation, SAMS

1 Introduction

In 2012, the Norwegian University of Science and Technology (NTNU) and the Swedish Polar Research Secretariat (SPRS) established a collaboration in polar research under the umbrella of the memorandum of understanding, “Nordic Cooperation in Polar Research”, signed on January 29, 2010. A manifestation of the collaboration between NTNU and SPRS includes a series of Arctic research cruises. In the autumn of 2015, NTNU and SPRS performed the third research cruise named the “Oden Arctic Technology Research Cruise 2015” (OATRC2015), which involved the two Swedish icebreakers, Oden and Frej, in the international waters north of Spitsbergen. The ExxonMobil Upstream Research Company supported and participated in OATRC2015.

The overall objective of OATRC2015 was to perform a safe cruise, collect valuable and important scientific data, and conduct full-scale field trials to test key technologies. The scientific scope of OATRC2015 included three major fields of study, namely: 1) collection of full-scale data necessary to build, calibrate and validate numerical models for floaters in ice, 2) collection of full-scale data necessary to build, calibrate and validate numerical models for ice management operations, and 3) collection of data relevant for health, safety and environmental research.

OATRC2015 was successful in its objectives and generated a considerable amount of environmental data, including ice, metocean, and biodiversity data, along with a unique dataset on icebreaker performance and ice management operations. An overview of the research conducted, and major findings are provided below.

In addition, the following text introduces a newly released Simulator for Arctic Marine Structures (SAMS), which is a product of NTNU’s spin-off company: Arctic Integrated Solutions AS (ArcISo). The text includes an extensive discussion on the use of OATRC2015 full-scale data to validate SAMS.

2 OATRC2015 Overview

The Swedish icebreakers, Oden and Frej, were used in the research cruise. Fig. 1 shows a picture of the two icebreakers conducting ice management trials in the Arctic Ocean during OATRC2015. Table 1 shows the technical specifications of the icebreakers. An AS-355NP helicopter was also used during the expedition, and flight operations were based off the Oden. During planning and preparation, both vessels and the helicopter operations were thoroughly reviewed and prepared for the expedition.

Fig. 1 Icebreakers Oden and Frej testing ice management tactics during OATRC2015.

Table 1 Technical data of Oden and Frej.

Oden	
Length	107.75 m
Beam	31.2 m
Draft	7.0-8.5 m
Total power	18 MW, 24500 hp
Speed in open water	15 knots, normal sea speed 11 knots
Crew	23 persons, up to 50 scientists
Icebreaking capability	1.9 m level ice at 3 knots
Bunker capacity	4600 m^3, equal to 27000 nmi in open sea at 13 knots or 100 days
Displacement	11000 – 13000 tonnes
Propulsion	4 medium speed, 8-cylinder Sulzer diesel engines. 2 propellers in nozzles
Building yard	Götaverken-Arendal AB 1988 (NB953)
Owner	Swedish Maritime Administration
Frej	
Length	105.7 m
Beam	23.8 m
Draft	8.3 m
Total power generators	25 000 hp
Speed in open water	18 knots, normal sea speed 12 knots
Crew	25 persons, up to 25 scientists
Icebreaking capability	1.2 m level ice at 3 knots
Bunker capacity Heavy fuel	1400 m3
Displacement	7800 t
Propulsion	2 front, 2 aft electric engines
Building yard	Helsinki Shipyard
Owner	Swedish Maritime Administration

Sixty-two scientists and supporting personnel participated in the research cruise. A full list of participating organisations is listed under the acknowledgements section in this paper. SPRS performed a medical risk assessment followed by a thorough medical screening of all participants with special focus on the remote Arctic operations.

The cruise began on the 18th of September 2015 from Longyearbyen, and the icebreakers returned to Longyearbyen on the 2nd of October 2015. Fig. 2 shows the complete timeline of OATRC2015. Fig. 3 displays the tracks of the two vessels during the research cruise. The two icebreakers generally followed the same pathway to the ice pack north of Svalbard while conducting some preliminary communications testing. However, on the return trip, the two icebreakers adopted different pathways due to an encroaching autumn storm system.

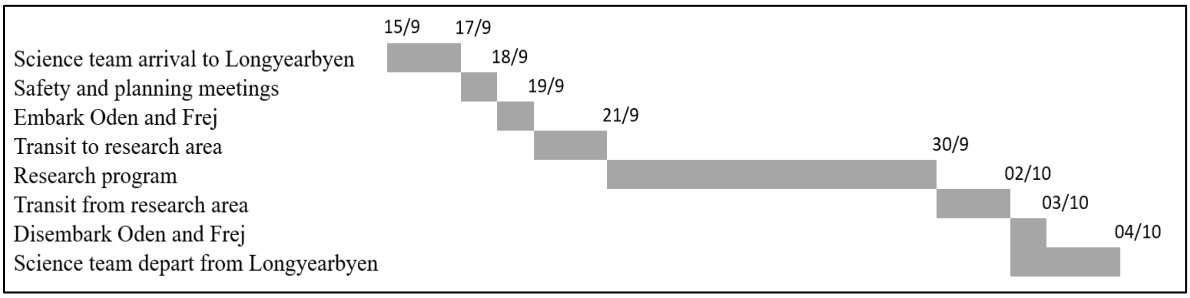

Fig. 2. OATRC2015 timeline.

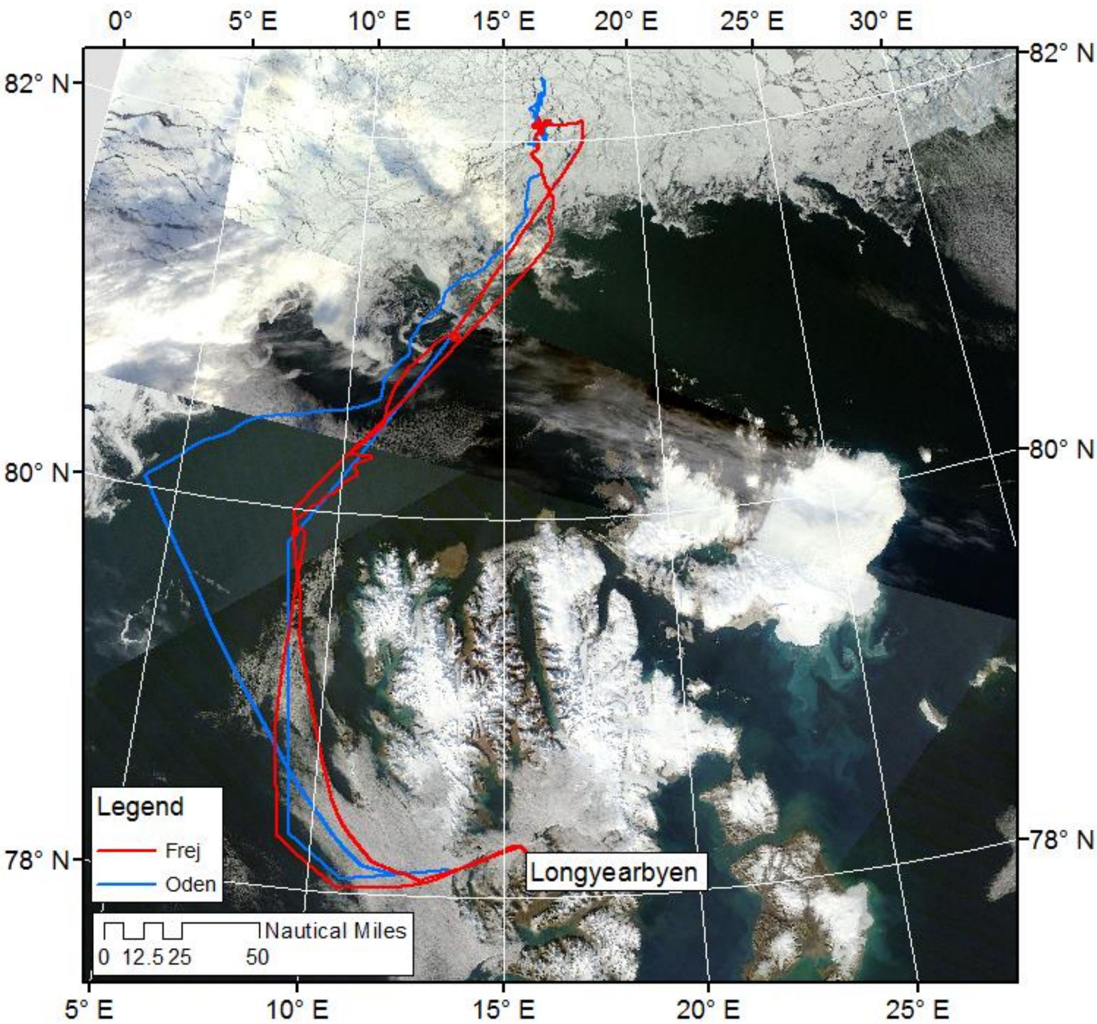

Fig. 3. Routes of the Oden and Frej: 18.09.2015 to 02.10.2015. NASA Worldview, (see Worldview).

Longyearbyen was used as the shore base for the expedition. Safety and planning meetings were held at the University Centre in Svalbard (UNIS) in the days prior to the expedition. UNIS provided safety oversight for OATRC2015, leading risk assessments and emergency planning and training, and on-board field safety experts. Loading of the equipment and vessel outfitting were conducted at Longyearbyen, Svalbard and at the vessels' home ports in Sweden.

The ice conditions on September 18, 2015 are shown in the background image of Fig. 3. Sea ice conditions suitable for the Frej to safely and effectively operate were specifically sought out for the trials. Hence, the trials were conducted in predominantly medium first-year ice, with an average thickness in the range of 0.7 to 1.2 m and mostly 9+ tenths ice concentration. The ice thickness was continuously measured in real time using Electro-Magnetic (EM) systems hung over the bow of each icebreakers (Fig. 4a). Such methods have been used in previous research expeditions (Haas et al., 2011). In addition to the EM system, a supporting ice thickness camera was also installed to visually extract the ice thickness information (Lu et al., 2016a). Both thin and thick first-year ice, as well as young ice and some older ice inclusions, were also occasionally encountered. Fig. 5 shows typical views of the ice conditions encountered.

A trace of the beacon-measured ice drift over the 14-day trials period is shown in Fig. 4b. This trace is the combination of two beacons deployed during OATRC2015. Most tests were conducted around a fixed waypoint (82° 4.65'N 16° 27.18'E). Local radio and satellite ice drift beacons were used to monitor ice drift during the trials, as well as long-term regional ice drifts. As shown in Fig. 4b, during the 14-day expedition, there were numerous Coriolis loops and cusps at approximate 12-hour intervals, and several 180° drift reversals in response to changing winds. Ice drift speeds during the period ranged from 0 to 0.4 m/s, with an overall average of approximately 0.2 m/s.

Apart from the storm event during the return transit, the general weather conditions were good, with varying visibility and low to moderate wind speeds. The air temperatures ranged between +4°C and -13°C. Helicopter operations were limited by weather on only a few occasions; however, some fog and snowfall were encountered, providing an opportunity to test the ice management operations and technology in conditions with reduced visibility.

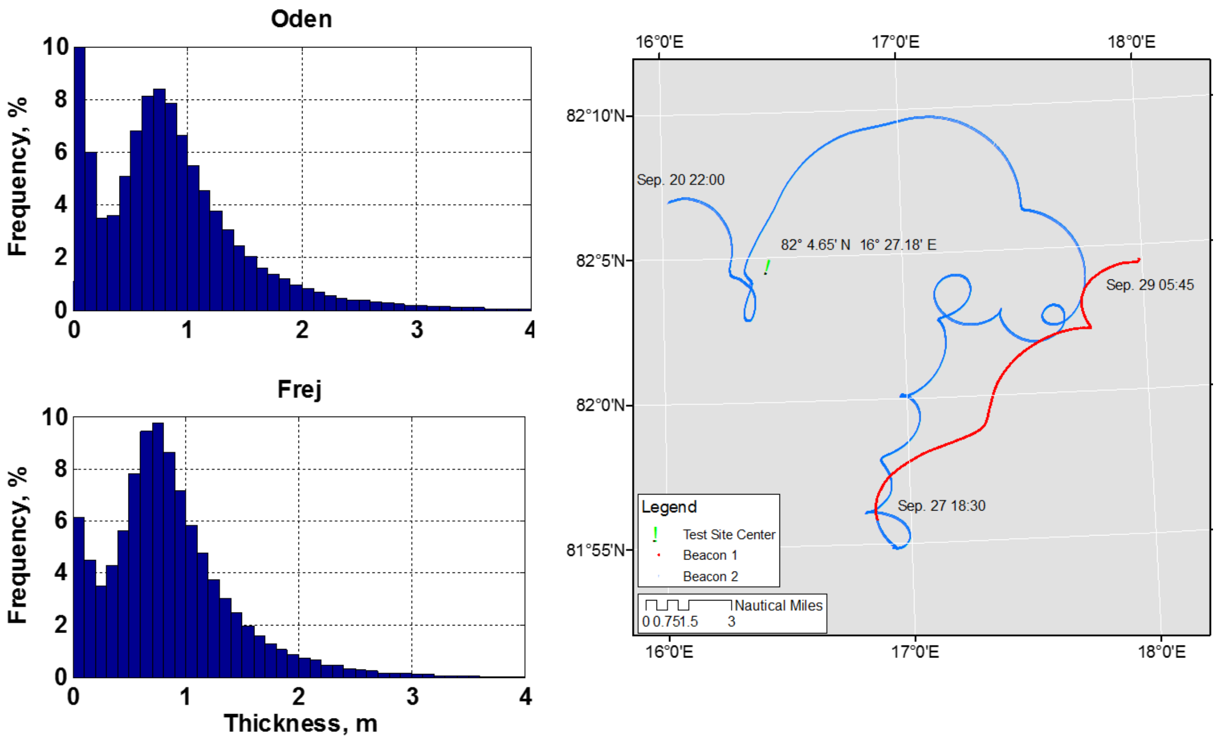

a) Ice thickness b) Ice drift

Fig. 4. Observed ice thickness and ice drift.

Fig. 5. Photos of typical ice conditions.

3 OATRC2015 Research Program

The scientific scope of OATRC2015 included three major fields of study:

- Collection of full-scale data necessary to build, calibrate and validate numerical models for floaters in ice,
- Collection of full-scale data necessary to build, calibrate and validate numerical models for ice management,

- Collection of data relevant to health, safety and environmental research.

Fig. 6 illustrates the scope of OATRC2015, and the numerous research activities that were performed during the 14-day field programme. This paper provides a brief description of the performed research. A detailed description of the activities can be found in the companion papers in this special issue.

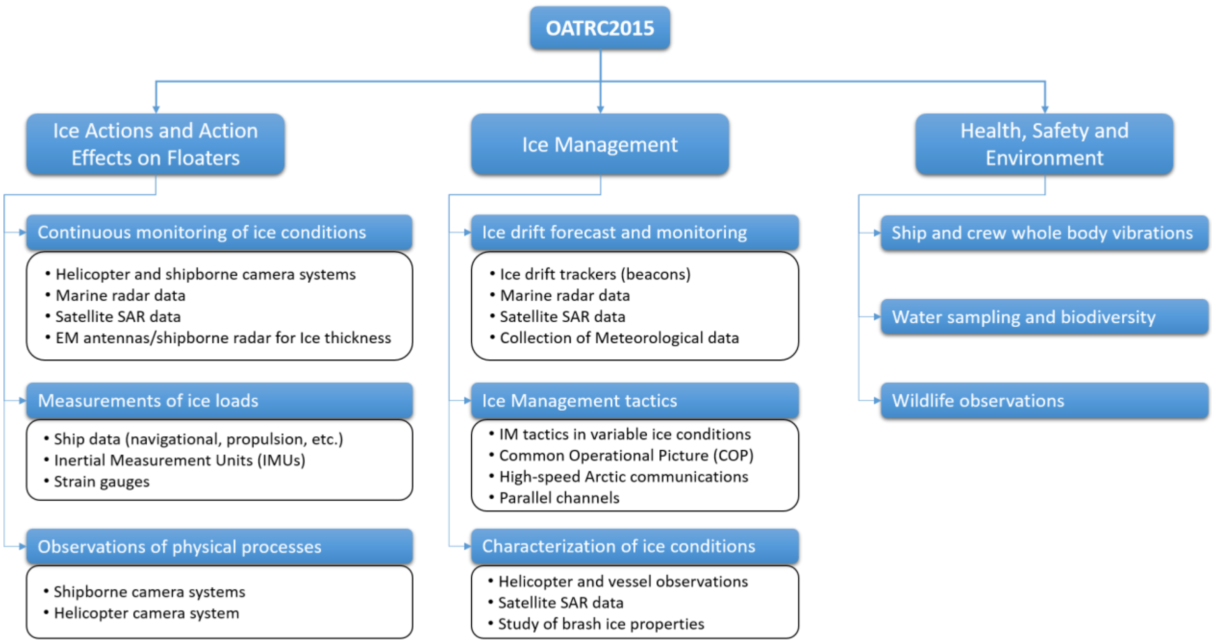

Fig. 6. OATRC2015 research activities.

3.1 Ice Actions and Action Effects on Floaters

One of the main objectives of OATRC2015 was to collect the necessary full-scale data to build, calibrate and validate theoretical models for estimating ice actions and action effects on floating structures. This included quantification of the sea-ice environment, observation of the ice-ship interaction processes, measurements of the local and global ice loads on the ship, and measurement of the ship response. Fig. 7 provides some example data collected under this research thrust.

3.1.1 Continuous monitoring of ice conditions and Observations of Physical Processes

Numerous cameras of three types were installed on Oden and Frej:

Type #1: Cameras to document the ice conditions (e.g., 360° camera, 180° camera, forward, aft);

Type #2: Cameras to observe ice-structure interaction zones (i.e., bow video cameras);

Type #3: Cameras to measure the ice thickness, wake region, parallel channel effect and floe motion.

Fig. 7a provides an example of the 180° imagery collected on the Frej. In Fig. 7a, the incoming ice conditions forward of the Frej are captured, and the Oden can be observed conducting ice management operations off the starboard side. These imagery data were used by Lu et al. (2016a) to estimate the ice concentration in real-time. Bow video cameras were very useful for observing the bow-ice interactions. The cameras produced important information on the physical processes of ice breaking and rotating for the two different bow shapes. Cameras were also used to observe the motion of ice floes in the propeller wake and to calculate drag forces (Tsarau, 2016; Tsarau et al., 2018).

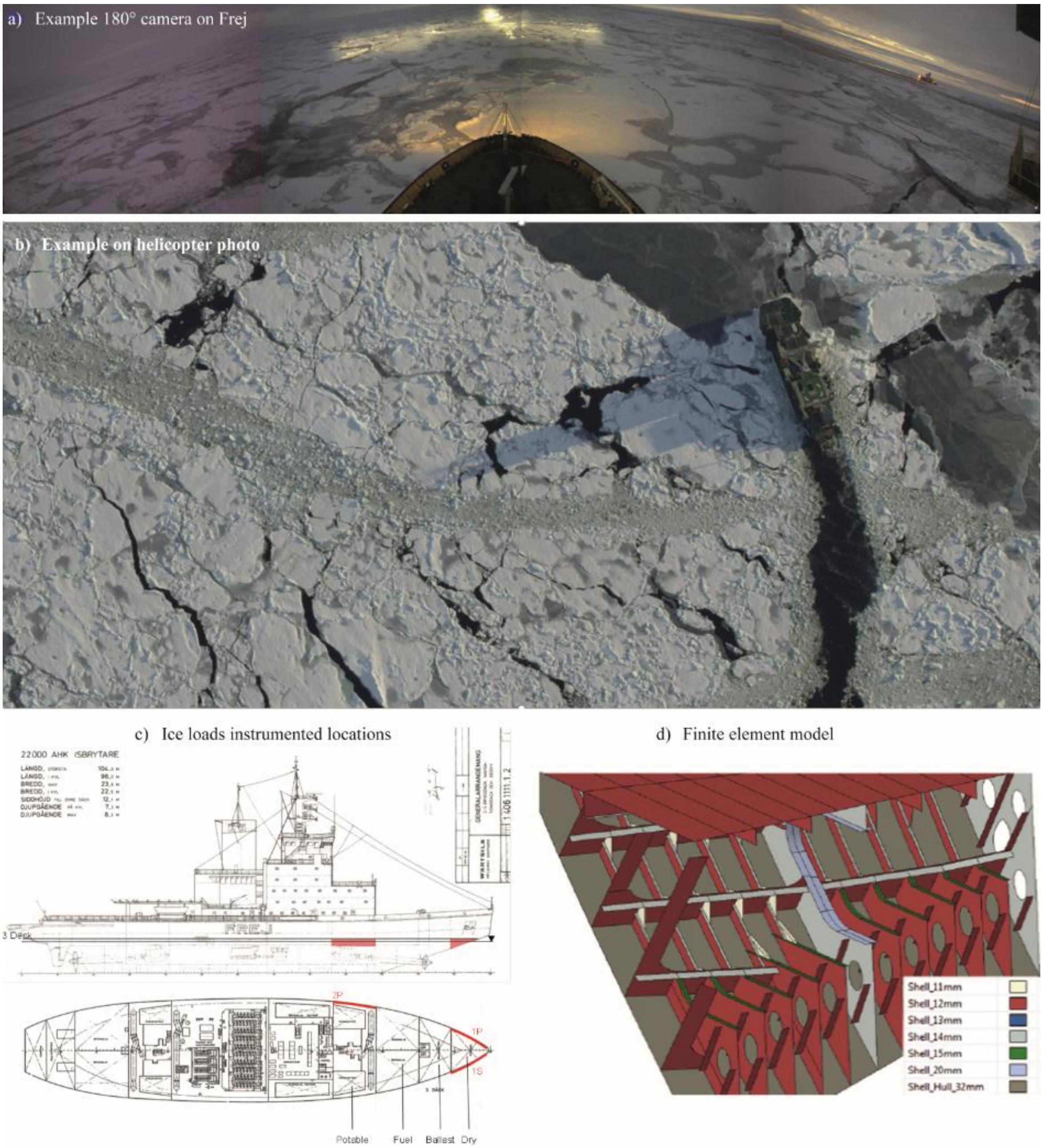

Fig. 7. Ice actions and action effects on floaters.

Furthermore, a total of 12 helicopter flights were conducted to document ice conditions using high-resolution photography. The AS-335NP helicopter was used for photographing, and it was equipped with a camera system consisting of a 6-axes gyro stabilised camera support (i.e., ShotOver F1) and a Red Dragon camera with Fujinon 25 – 300 mm lens. All the images were enriched with real-time information, such as latitude, longitude, and the camera's filming parameters (i.e., pan, tilt and roll angles). Fig. 7b provides an example of the imagery collected during OATRC2015. In Fig. 7b, the Oden can be seen passing perpendicularly through an existing ice management channel. A small unmanned aerial system (UAS) was also tested for the collection of aerial photography near the Frej. The UAS collected limited data, as flight operations were challenged by the marine Arctic conditions.

Finally, ice enhanced marine radar was used on both icebreakers to monitor the local ice conditions and ice drift (Shafrova et al., 2016). As noted above, EM instruments were deployed on both icebreakers to measure the ice thickness. The use of a radar system to monitor ice thickness was also tested during the expedition.

3.1.2 Measurement of ice loads

The Oden's and the Frej's navigational and propulsion data (e.g., position, heading, speed over ground, shaft power, propeller RPM and pitch, rudder angles) were continuously logged. These data in combination with the data collected on ice conditions (e.g., ice thickness, floe size distribution, concentration) are very useful to analyse the performance of the two vessels in different ice conditions.

The vibrations of the Oden and Frej due to ice actions were measured with inertial measurement units (IMUs). On each icebreaker, 4 IMUs were placed close to the ice interaction zone. Each IMU contained six sensors, i.e., three accelerometers and three gyros, measuring the six degrees of freedom (6DOF) motion of the ship. This enables the calculation of global ice loads on the vessels, see Kjerstad and Skjetne (2016). The IMU data are also useful to study the different ice failure modes and possibly to anticipate changes in ice drift direction (Heyn and Skjetne, 2016). Heyn and Skjetne (2018) applied the Wigner-Ville distribution on the ice-induced acceleration measurements, which gives time-varying energy spectral densities and significantly improves the frequency analysis of the ice-load signals. They provided examples of different ship-ice interaction events, which underline that the time-frequency distribution can be used to identify different ship-ice interaction events and to evaluate the severity of ice actions on the ship.

A system was designed and installed on the icebreaker, Frej, to measure the local ice loads on the vessel (Piercy et al., 2016). The system consisted of an array of over 160 strain gauges installed over three panels on the bow and shoulder of the vessel. The instrumented locations are shown in Fig. 7c. Physical calibrations onsite were performed as quality checks on the gauge installation and to benchmark the finite element model (Fig. 7d) used to convert the measured strain data into pressures. More than 200 hours of ice loads data were collected throughout the programme, including measurements while station-keeping in managed ice conditions, actively managing ice, and transiting. Fenz et al. (2018) used the up-crossing rate method to analyse the local pressure data from the Frej. They concluded that the local pressures from station-keeping in managed ice are two to four times lower than the transiting cases. They claimed that such a finding provides a sound basis for advocating for local design pressures that are lower than the current recommendations, which can potentially extend the operating envelope of offshore vessels, leading to significant savings.

3.2 Ice Management

One of the main objectives of OATRC2015 was to collect full-scale data necessary to build, calibrate and validate theoretical models for ice management (IM) operations. This includes: forecasting and monitoring of ice drifts, performing IM tactics in various ice conditions, and monitoring outgoing ice conditions resulting from different ice management scenarios. Fig. 8 provides example data collected under this research thrust.

3.2.1 <u>Ice drift forecasting and monitoring</u>

Ice drift beacons were used to provide input to ice management field operations and to study long term regional ice drift. Both locally transmitting radio and satellite Iridium beacons were used. Fig. 4b shows example drift data collected during the campaign. The drift data were also used to benchmark satellite methods for monitoring ice drift and to test tactical ice drift forecasts. Fig. 8a provides example regional ice drift information extracted from the Sentinel-1 satellite imagery.

Mitchell and Shafrova (2018) describe a free drift tactical ice forecast model, developed by the ExxonMobil Upstream Research Company (EMURC) and designed to forecast the drift of individual ice floes in low ice concentrations. The model was applied in near real time during OATRC2015. Mitchell and Shafrova (2018) compare the forecast results with the drift data collected during OATRC2015. The results show that the free drift forecasting tool produces reasonably accurate and useful forecasts in the high concentration ice observed.

3.2.2 <u>Ice management tactics</u>

Various icebreaker fleet deployment tactics were tested during OATRC2015. During these tests, the Oden and Frej were deployed in systematic ice management patterns around a stationary waypoint to assess the resulting managed ice conditions. Approximately 150 hours of ice management tests were conducted, with the longest test lasting approximately 90 hours. The systematic commands for the two icebreakers were communicated using a Common Operational Picture (COP). The COP was used to analyse incoming ice conditions and generate ice management commands for display on the bridge of both icebreakers. Fig. 8b shows orbital ice management tactics on the icebreaker captains' view of the COP. In this test, the Oden was acting as the primary icebreaker, following the largest diameter orbital path around the fixed waypoint. The Frej was acting as the secondary icebreaker, further reducing the floe size in a smaller orbital pattern around the fixed waypoint. Ice management tactics and COP are further discussed by Hamilton et al. (2016) and by Shafrova et al. (2016), respectively.

Kinematic simulations were used to design the systematic arched racetrack tactics that were implemented and tested during OATRC2015. Holub et al. (2018) compared the simulation results with the data from OATRC2015. They showed that the virtual drilling rig was maintained within the managed ice channel in complex ice drift conditions that included multiple ice drift loops, cusps, and reversals; which confirm the fundamental simulation methods.

Omnidirectional radio antenna units (KM Seatex MBR 179) were installed on both the Oden and Frej to ensure a high bandwidth data link for IP-based video streaming, VoIP, and data communication between the vessels. In addition, a customised Gb-WiFi inter-vessel network was configured and installed on both vessels. The inter-vessel communication between the icebreakers was systematically tested, and the performance of the MBR link and WiFi link were compared. During the 14-day programme, the MBR link worked robustly, without any fallouts, giving a data rate of approximately 380 MB/s. The WiFi-link, on the other hand, had a shorter range, but gave higher speeds at lower output power.

3.2.3 <u>Characterisation of ice conditions</u>

During ice management operations, a narrow parallel channel spacing can effectively reduce ice floe sizes at the protected vessel/structure. However, a channel spacing that is too narrow might lead to excessive, or even impractical, ice management operations. During OATRC2015, several parallel channel tests were conducted. Fig. 8c shows a typical snapshot of the ice conditions while carrying out parallel channel tests. An image processing technique was used to extract information about the cracks that formed between the neighbouring parallel channels. Crack orientation and occurrence frequency were quantified versus different channel spacing to reveal the relationship between the parallel channel spacing and the size of the generated ice floes during an IM operation (Lu et al., 2016b). Lu et al. (2018a) presented a theoretical model for parallel channels' fracturing mechanism during ice management operations, and Lu et al. (2018b) used full-scale data from OATRC2015 to validate that model.

Satellite data of various forms were used 1) to prepare for the expedition and site selection, 2) to monitor ice conditions and experimental results during the field campaign, and 3) for ice monitoring following the trials. The satellite data used at different stages of OATRC2015 cover a wide spectrum ranging from ultra-high-resolution images (e.g., WorldView 3 optical satellite imagery with 30 cm resolution and CosmoSkyMed X-band radar satellite imagery with 1.0 m resolution) to lower resolution images (e.g., AQUA/TERRA MODIS optical satellite imagery with 250 m resolution and 40 m resolution Sentinel-1 C-band radar imagery). Matskevitch et al. (2016) reports that 228 satellite images were acquired and analysed in support of OATRC2015.

The properties of the brash ice produced during IM were tested repeatedly. Each test took approximately 10 minutes, and it measured the brash ice thickness, friction at uplift and weight of ice blocks. The experimental setup is shown in Fig. 8d, and it can be described as an umbrella, 2 m in diameter and 3 m in height. In total, 18 tests were performed, measuring brash ice properties at 14 different locations. The measured brash ice thicknesses were between 0.6 m and 1.3 m, which is in good agreement with the EM-measurements. The peak load at uplift was typically twice the weight of the ice for interlocked ice blocks and very small for free-floating blocks. The data from the brash ice tests will be used later to verify numerical models of brash ice.

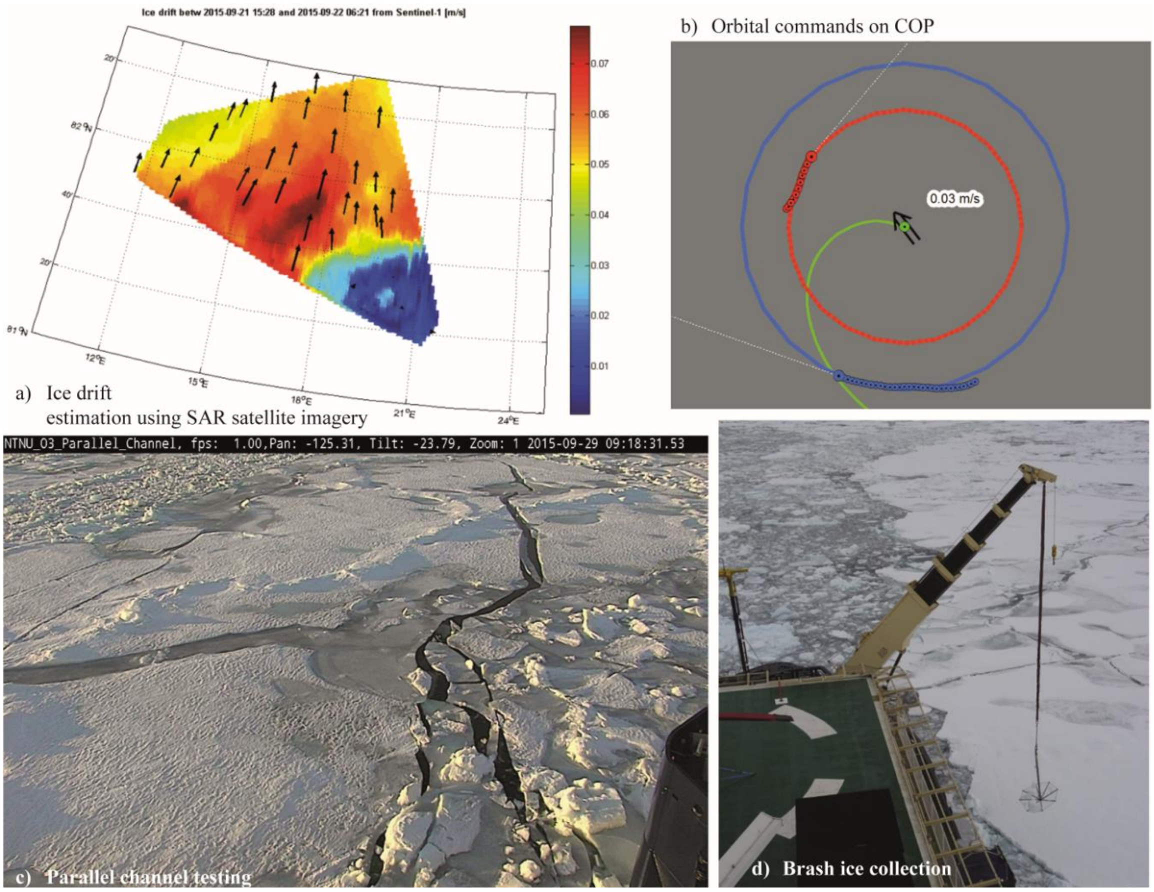

Fig. 8. Ice management.

3.3 Health, Safety, and Environment

One of the main objectives of OATRC2015 was to collect data for health, safety, and environment research. This included data on ship and crew vibrations during icebreaking operation, water collection and processing to understand marine biodiversity, and wildlife observations.

3.3.1 Ship and crew vibrations

The level of exposure to whole body vibrations for the Oden and Frej crew during icebreaking conditions were measured. The purpose of this measurement was to investigate whether problems with the lower back are more common among icebreaker crew members. The methods used in the study include a variety of physical measurements and a questionnaire (Johannesson, 2016), see Fig. 9a.

3.3.2 Water sampling and biodiversity

A total of 9 stations and 12 casts were performed with the Oden´s CTD (Conductivity, Temperature, and Depth) (see Fig. 9b) to collect hydrographic data and sample water from different depths. The system used was a SeaBird

911+ with 11+ deck unit CTD equipped with 23 Niskin bottles of 6 litres each. The measured parameters were: temperature (°C), salinity (psu), oxygen content (ml/L), conductivity (S/m) and sound velocity (m/s). Samples were taken for biological analyses of bacteria, chlorophyll, nutrients, and pigments. Typical depths for samples were bottom, 225, 40, 25 and 10 metres.

The seawater samples were also used for environmental genomics analysis. Environmental genomics is an evolving technology area that is used to characterise biodiversity in a survey region by analysing the environmental DNA in environmental media, such as seawater or sediment (N’Guessan et al., 2012; Baird and Hajibabaei, 2012). In addition to samples collected using the CTD, the samples were also collected using the Oden’s underway system throughout the journey. Once the seawater samples are processed and analysed, the DNA sequence data will be compared to a genomic database and will allow for the identification of known and potentially unknown marine organisms. These data will then be validated against marine mammal observations made by the Marine Wildlife Observers (MWO) who were also present on the vessel (see Table 2).

Fig. 9. Health, Safety and Environment.

Table 2. Marine wildlife observations

Marine mammal species	**Total individuals**	**Total observations**		**Bird species**	**Hours observed**
Blue whale	3	2		Fulmar	53
Fin whale	6	5		Pomarine jaeger/skua	2
Minke whale	4	4		Arctic jaeger/skua	1
Unidentified large whale	4	3		Ivory gull	110
Orca	7	2		Glaucous gull	27
Bearded seal	2	2		Kittiwake	37
Hooded seal	8	5		Arctic tern	1
Ringed seal	4	3		Brünnich's guillemot	11

Harp seal	2	1		Puffin	4
Unidentified seal	15	12		Black guillemot	26
Polar bear	9	7		Little auk/dovekie	9
Unspecified mammal	5	3		Snow bunting	5
Total	69	49		Total	286

4 Simulator for Arctic Marine Structures (SAMS)

As offshore activities in the Arctic constitute a relatively new field, with only a handful of relevant operations to draw experience from, and since full-scale trials are extremely expensive, there is an expressed need for much more extensive, detailed and cost-efficient analysis of concepts based on numerical simulations. However, until recently, simulation tools of sufficient quality to perform such numerical analysis have not existed. The only verification available has been through a limited set of experiments in ice model basins. Today, this has changed, partly through the efforts at NTNU hosting SAMCoT (Centre for Research-based Innovation - Sustainable Arctic Marine and Coastal Technology), laying the foundation of a versatile and highly accurate high-fidelity numerical simulator for offshore structures in various ice conditions, such as level ice, broken ice and ice ridges.

Arctic Integrated Solutions AS (ArcISo) is a spin-off company from NTNU, established in 2015 with the vision of increasing the technology readiness level of SAMCoT's numerical models to become a professional software package for the analysis of sea ice actions and action effects on Arctic offshore structures. This software package is now called the Simulator for Arctic Marine Structures (SAMS), and it was first released in 2017. The following text briefly introduces the theoretical basis of SAMS, and it discusses the potential use of OATRC2015 full-scale data to validate the simulator. Recall that one of the major objectives for OATRC2015 was to collect the necessary full-scale data to build, calibrate and validate numerical simulators for floaters in ice.

4.1 Theoretical Basis for SAMS

This section gives only a brief description of the theoretical basis for SAMS. More details can be found in numerous earlier publications. An overview paper, which gives a thorough description of the theory and software implementation of SAMS, is in progress and will be submitted for publication soon.

Depending on the confinement, ice concentration and floe size distribution, the governing mechanisms during the floe ice and floaters interactions can differ considerably. The term floe ice is quite generic, and can be used to describe level ice or any fragmented ice field whether it is naturally broken, e.g., by gravity waves, or artificially broken, e.g., by ice management (IM) operations.

For the numerical modelling of a floater in floe ice, time-domain modelling is inevitable due to the considerable nonlinearities in the interaction processes between ice floes and the floater. The distinct nature of ice floes in a broken ice field has often promoted the use of discrete element modelling methods (DEM). The latter can broadly be divided into two main categories: smooth discrete element modelling (SDEM) and non-smooth discrete element modelling (NDEM). The difference between the two can be seen as the difference between implicit and explicit time integration, allowing much larger time steps, while maintaining stable simulations, when using NDEM. SAMS falls under the NDEM category, but it applies a novel implicit time stepping scheme and an improved contact model, enabling general visco-elastic contacts. This increases the accuracy and expands the applicability range of the SAMS compared to existing models, see Van den Berg et al. (2017).

Moreover, the current version of SAMS adopts an analytical framework that supplements the NDEM method with analytical closed-form solutions to simulate the fracture of sea ice. This methodology was first presented by Lubbad and Løset (2011) to model the bending failure of ice. Later, the method was expanded with a number of closed-form solutions that cover other failure modes, e.g., splitting and radial cracking. These solutions are published in a series of papers (Lu et al., 2015a; Lu et al., 2015b; Lu et al., 2016c).

In addition to the improved NDEM formulation and the comprehensive set of analytical solutions to ice fracture, SAMS applies innovative numerical solutions to calculate different hydrodynamic force components on the floater and every ice floe in the calculation domain. This includes, among other things, drag forces from wind, current and propeller flow. These solutions are calibrated and validated against full-scale and lab-scale data, see (Tsarau et al., 2014; Tsarau and Løset, 2015).

Fig. 10 illustrates the aforesaid building block of SAMS, namely: 1) the NDEM or multi-body dynamics module, 2) the fracture module, and 3) the hydrodynamic module. Additional information on these modules is given below.

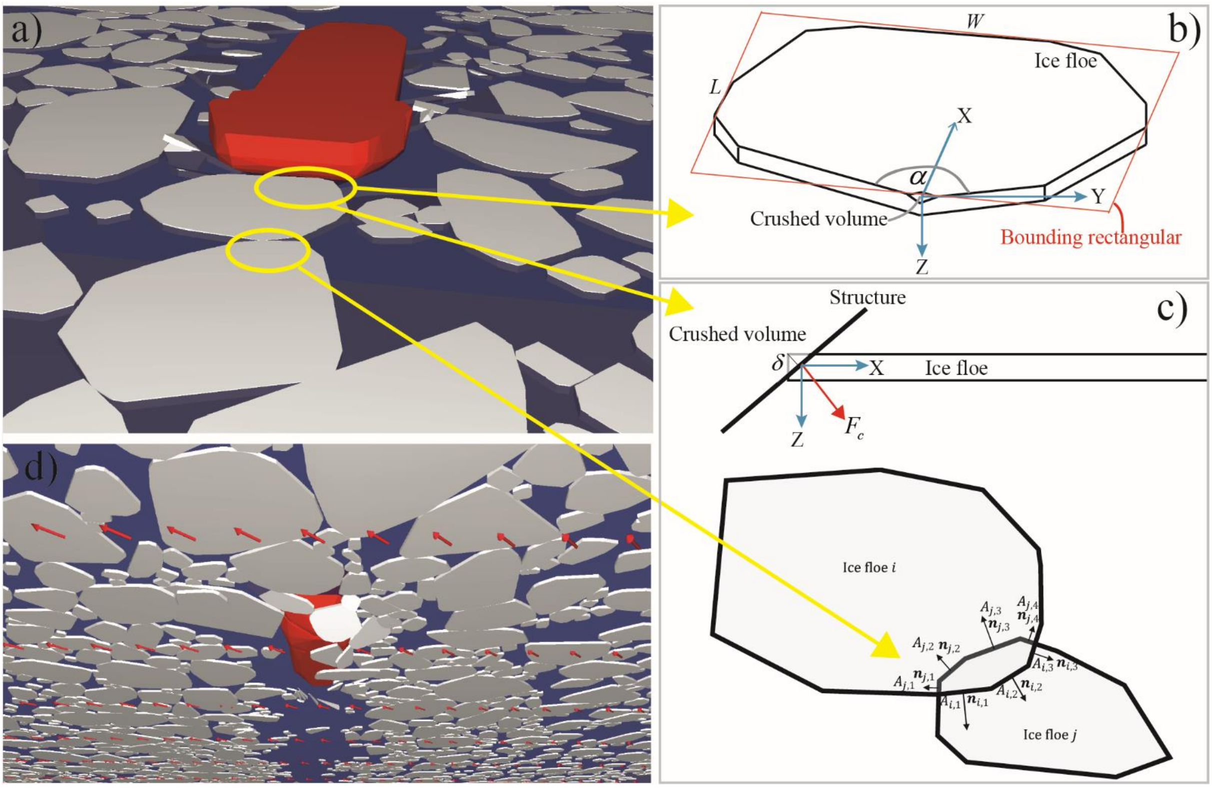

Fig. 10. Illustration of different modules within SAMS: a) the simulation environment; b) the fracture module; c) he NDEM or multi-body dynamic module illustrating the non-rigid contact due to ice crushing at the contact interface; d) illustration of the fluid domain, e.g., current flow, with velocity vectors.

4.1.1 <u>Multi-body dynamic module and contact model</u>

As described in the previous section, a floe ice field is represented numerically in the simulator as a collection of discrete ice bodies. The interaction forces at ice-ice and ice-structure contacts are calculated using an implicit time-stepping scheme that falls under the category of NDEM modelling. Previously, the NDEM modelling technique was applied by several researchers to model ice-structure interactions, e.g., (Alawneh et al., 2015; Dudal et al., 2015; Konno and Mizuki, 2006; Lubbad and Løset, 2011; Metrikin, 2014; Yulmetov et al., 2016). Within the framework of NDEM modelling, one of the key challenges is obtaining a physically correct contact force. The 'traditional' NDEM methodology only defines contact impulses, which cannot be easily translated to equivalent contact forces. This is problematic because the contact force is needed to determine whether ice failure will occur. Earlier works partly mitigated this limitation by defining an upper limit to the contact force based on the contact geometry and material properties, as is done in Lubbad and Løset (2011) and Metrikin (2014), in which both papers used a different method to limit the contact force. Others attempted to obtain a contact force by post processing of the obtained contact impulses, as is done by Yulmetov et al. (2016) and Alawneh et al. (2015).

SAMS uses the novel method presented by Van den Berg et al. (2017) to remedy the abovementioned problem. This method considers the contact crushing force as well as the force-penetration gradient, leading to a more accurate contact force prediction than with previously applied methods for the majority of contact cases. The contact model in SAMS assumes constant energy absorption per unit crushed volume of ice, represented by a Crushing Specific Energy value (CSE). This is in accordance with previous research (Kim and Gagnon, 2016; Kinnunen et al., 2016), and it is equivalent to a contact model with constant crushing pressure. This contact model ensures that the energy absorbed in an ice-ice or ice-structure contact matches the change in overlap volume of the interacting bodies within each time step, where the overlap volume of interacting bodies represents crushed ice.

The energy match is ensured by considering the projected area of a contact occurring, and the expected change of projected area. This is used to define a force-penetration gradient, as in Eq. (1).

$$\frac{\Delta F}{\Delta \delta} = \left(\frac{\left(A_{\mathrm{proj}}^{\mathrm{prop}} - A_{\mathrm{proj}} \right) \mathrm{CSE}}{\Delta \delta} \right) \qquad (1)$$

where $A_{\mathrm{proj}}^{\mathrm{prop}}$ stands for the projected area when the interacting bodies are propagated with their current velocity, A_{proj} is the contact projected area at the beginning of the time step, $\Delta\delta$ is the change of contact penetration, and $\Delta F / \Delta\delta$ is the force-penetration gradient. This force-penetration gradient is used together with the projected area at the beginning of the time step to define the compliance parameters that represent local ice crushing.

Three types of contact behaviour can be distinguished as follows:

1. **Crushing contact**. The increase in overlap volume of interacting bodies is matched by the energy dissipated during the contact.
2. **Resting contact**. The relative velocity between the interacting bodies is zero. The contact force is determined such that the resting contact is maintained, provided that the crushing force is not exceeded, and the force needed to maintain the zero velocity is not negative (no adhesive force).
3. **Separating contact**. The contact penetration decreases, and the contact force drops to zero.

This contact behaviour can be considered as hysteretic damping, in which the loading/unloading curve will be similar to Fig. 11. A more detailed description of the contact model can be found in Van den Berg et al. (2017).

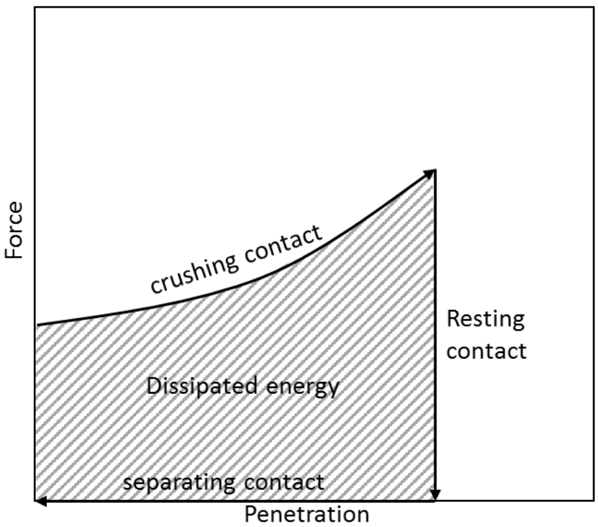

Fig. 11 Crushing contact implementation as hysteretic damping.

4.1.2 **Floe ice's fracture module**

The ice fracture module aims to simulate the fracturing of ice floes during the interaction with the floater. Previously, we investigated two different approaches to simulate ice fracture, i.e., a pure computational mechanics approach suitable for detailed design simulation, and a pure analytical approach targeting efficient simulations related to large scale Arctic marine operations.

The current version of SAMS implements the analytical fracture approach. The implemented algorithms can simulate local bending and global splitting failures of an ice floe interacting with the floater. The theoretical basis of these algorithms can be found at (Lubbad and Løset 201, Lu et al., 2015a; Lu et al., 2015b; Lu et al., 2016c).

Fig. 10a shows an illustration of an ice floe in contact with the floater. Basically, we employ Eq. (2) to calculate the contact force component F_Z that is needed to initiate the local out-of-plane bending failure (Note the coordinate system in the figure).

$$F_Z = \begin{cases} \dfrac{\sigma_f h^2}{3}\tan(\dfrac{\alpha}{2})[1.05 + 2\dfrac{\delta}{\ell} + 0.5(\dfrac{\delta}{\ell})^2] & (\alpha \le 90) \\ \dfrac{m\sigma_f h^2}{3}\tan(\dfrac{\alpha}{2m})[1.05 + 2\dfrac{\delta}{\ell} + 0.5(\dfrac{\delta}{\ell})^2] & (90 < \alpha \le 180) \end{cases} \quad (2)$$

in which,

σ_f is the flexural strength of sea ice, [kPa];

h is the thickness of sea ice, [m];

α is the angle of the wedge where the local bending failure occurs, also see

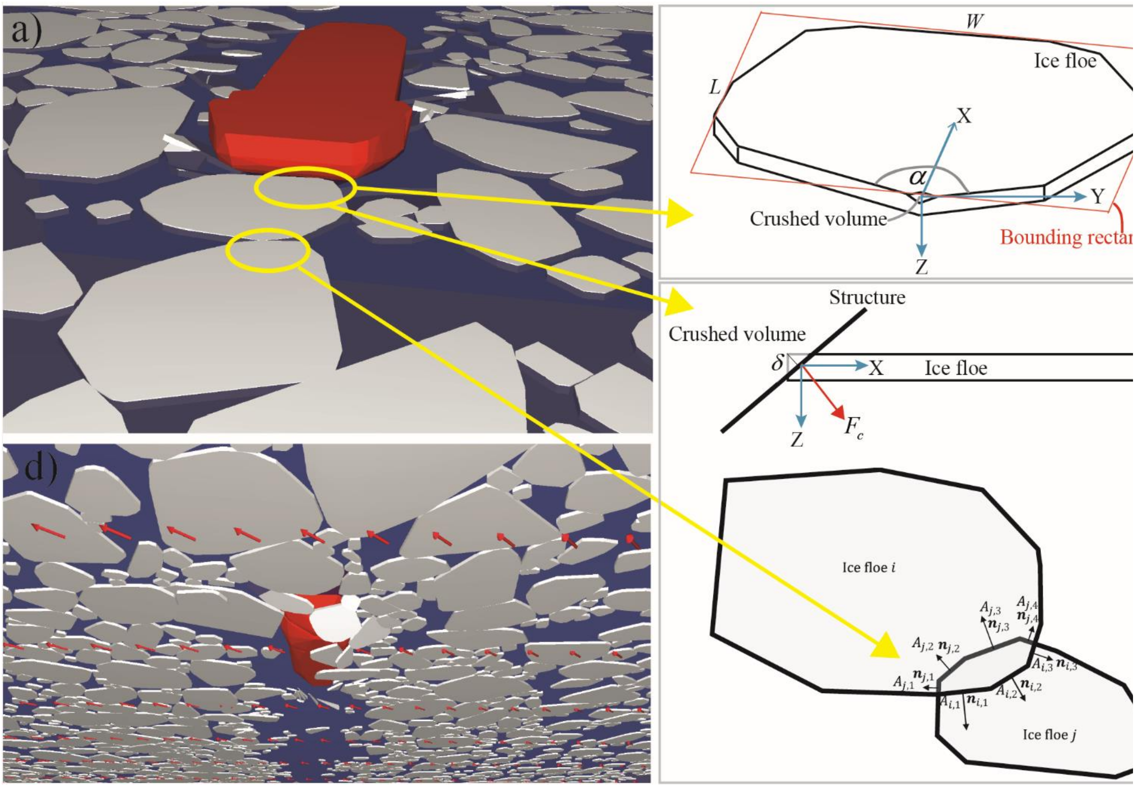

Fig. 10b, in [deg];

δ is the penetration depth and is considered equivalent to the loading area size at the wedge tip, [m];

m is the number of wedges that are bent off from the original ice sheet and is set as a random number between 2 and 3.

ℓ is the characteristic length [m] of sea ice and is calculated by $\ell = [Eh^3 / (12\rho_w g)]^{1/4}$, and E, ρ_w and g are the Young's modulus [kPa], water density [$\mathrm{kg/m^3}$] and gravitational acceleration [$\mathrm{m/s^2}$], respectively.

For the in-plane splitting failure mode, we have two cases: 1) centric or almost centric contacts, 2) and off-centre contacts. For the former, the fracture module employs Eq. (3) to calculate the contact force component F_Y that is needed to initiate the splitting failure. The ice floe is idealised by its bounding box with a length L and width

W , as illustrated in

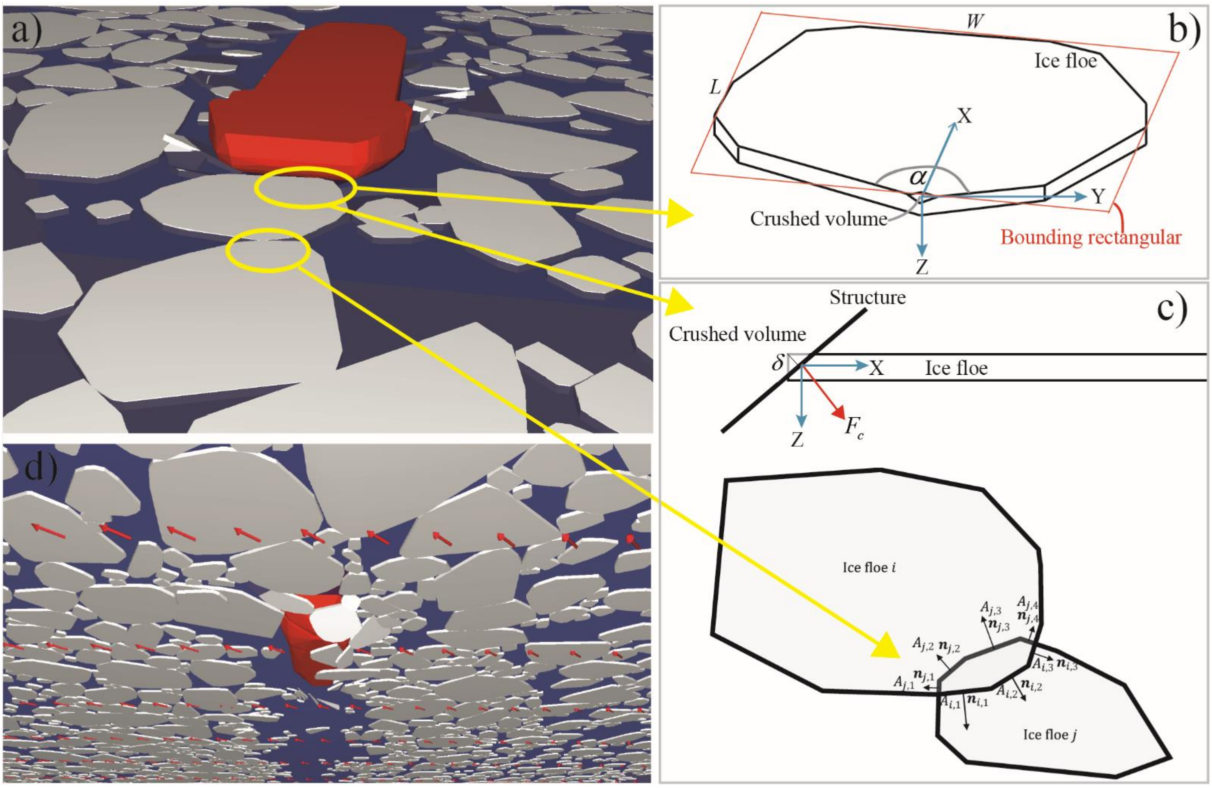

Fig. 10b.

$$F_Y(a) = \frac{hK_{IC}\sqrt{L}}{H(a,0)} \tag{3}$$

in which,

h	is the thickness of sea ice, [m];
K_{IC}	is the fracture toughness of sea ice, [$\mathrm{kPa}\sqrt{\mathrm{m}}$];
$H(a,0)$	is the weight function of a rectangular ice floe with a centred edge crack. Its formulation can be found in Dempsey and Mu (2014)
a	is the non-dimension crack length given by $a = A/L$, whereas A is the crack length and L is the length of the ice floe, as shown in Fig. 10b.

For off-centre collision cases, Eq. (4) is applied to calculate the F_Y that is needed to initiate the splitting failure. These equations are derived by Lu et al. (2018a), and they take into account the crack's kink behaviour.

$$F_Y = \frac{f(A_0/W_1)}{hK_{IC}\sqrt{W_1}}$$
$$f(A_0/W_1) = \sqrt{\frac{\pi}{\pi^2-4}}(\frac{A_0}{W_1})^{-1/2} + \sqrt{6}[1+\frac{0.3532}{(A_0/W_1)^{1/2}}+\frac{0.0116}{(A_0/W_1)^{1}}](\frac{A_0}{W_1}) \quad (4)$$

In Eq. (4),

h is the thickness of sea ice, [m];

A_0 is the length of the initial radial crack due to local bending failure, in [m]; it can be calculated as $A_0 = 2(D/k)^{0.25}$ with flexural rigidity D and the elastic foundation k of a floating ice floe, which can further calculated as $D = Eh^3/[12(1-v^2)]$ and $k = \rho_w g$ with Young's modulus E, Poisson's ratio v, water density ρ_w and gravitational acceleration g.

W_1 is the distance from the contact point to the closest free edge. As shown in Fig. 10b, the width of the bounding box $W = W_1 + W_2$ and $W_1 < W_2$. In general, it is required that $W_2 \geq 1.5 \cdot W_1$ for Eq. (4) to be valid. Otherwise, Eq. (3) is a better approximation.

For every time step, the multi-body dynamic (MBD) module detects the contacts, creates contact manifolds and calculates contact forces F_c. The fracture module calculates the failure criteria, as explained above, i.e., F_Z and F_Y. With this information available, the failure mode for each ice floe at each time step can be estimated according to Eq. (5),

$$\begin{cases} F_c \cdot \mathbf{z} \geq F_Z \text{ and } F_c \cdot \mathbf{y} < F_Y & \rightarrow \text{bending failure} \\ (F_c \cdot \mathbf{z}/F_Z) > (F_c \cdot \mathbf{y}/F_Y) \geq 1 & \rightarrow \text{bending failure} \\ (F_c \cdot \mathbf{y}/F_Y) \geq (F_c \cdot \mathbf{z}/F_Z) \geq 1 & \rightarrow \text{splitting failure} \\ F_c \cdot \mathbf{z} < F_Z \text{ and } F_c \cdot \mathbf{y} \geq F_Y & \rightarrow \text{splitting failure} \\ F_c \cdot \mathbf{z} < F_Z \text{ and } F_c \cdot \mathbf{y} < F_Y & \rightarrow \text{No failure} \end{cases} \quad (5)$$

in which, $\mathbf{z}$ and $\mathbf{y}$ are directional cosine in the vertical (z) and horizontal (y) directions, respectively. With this formulation, multiple failure modes can be achieved in the simulation, which gives more physically sound and realistic results. Fig. 12 demonstrates such coupling between local bending and global splitting failure modes in an off-centre collision scenario.

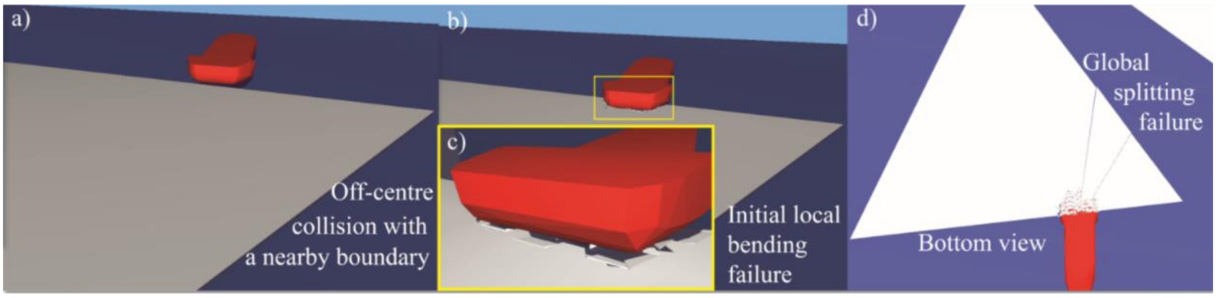

Fig. 12. Coupled local bending and global splitting failure modes in an off-centre collision case.

After ice breakings, the broken ice pieces are transported around the ship's hull (see Fig. 12d) and further interaction with the hull (structure) occurs. This is handled by the contact model described previously. In terms of simulation efficiency, built upon the MBD module, the current fracture module's analytical nature enables us to simulate unprecedentedly large temporal and spatial scales with satisfactory efficiency and accuracy.

4.1.3 <u>Hydrodynamics module</u>

Because all the interaction processes between the ice and structure occur within a fluid domain, the effect of hydrodynamics are present. For the current SAMS implementation, aside from the basic buoyancy of all bodies, the hydrodynamic forces, including the force due to the propeller flow, upon each individual ice floe and the structure are assigned explicitly, and ice drift simulations are possible given wind and/or current conditions. The total hydrodynamic force on a rigid body is considered here as a combination of the so-called form drag and skin-friction drag. The form drag arises because of the shape of the body, and follows the quadratic drag equation. It is higher for bodies with a larger presented cross section, and increases with the square of the flow velocity. The skin friction is caused by the viscous forces in the boundary layer at the body/fluid interface, and it is directly related to the wetted surface of the body, and rises with the square of the velocity component parallel to the wetted surface.

For an arbitrary rigid body in the presented simulator, the total hydrodynamic force is obtained by integrating the two drag components over the body's surface. A triangular mesh, as shown in Fig. 13, may be used to discretise the body's surface, which is useful for both the representation of the body's geometry and the calculation of the hydrodynamic forces. For the latter, the sum of the drag forces on the wholly immersed triangles is obtained as follows:

$$\mathbf{F}_h = \sum_{k=1}^{M} \left[\rho_w C_f S^k \,|\, \mathbf{U}_{\parallel}^k \,|\, \mathbf{U}_{\parallel}^k - \left(\frac{1}{2} \rho_w C_d S^k \left[(\mathbf{U}^k \cdot \mathbf{n}^k) \right]^2 \mathbf{n}^k \right) \Big|_{(\mathbf{U}^k \cdot \mathbf{n}^k)<0} \right] \tag{6}$$

where $\mathbf{F}_h$ is the total hydrodynamic drag force on the rigid body; M is the number of the wholly immersed triangles on the body's surface; ρ_w is water density; S^k is the surface area of the k-th triangle; $\mathbf{U}^k$ is the relative fluid velocity at the geometrical centre of the triangle; $\mathbf{n}^k$ is a unit vector normal to the triangle and pointing outwards from the body's interior; $\mathbf{U}_{\parallel}^k$ is the tangential velocity calculated as $\mathbf{U}_{\parallel}^k = \mathbf{U}^k - (\mathbf{U}^k \cdot \mathbf{n}^k)\mathbf{n}^k$; and, finally, C_f and C_d are the drag coefficients due to skin friction and pressure, respectively. The expression in parentheses in Eq. (6) is calculated only if $\mathbf{U}^k$ points towards the body's interior; otherwise it is 0. The moment due to the force $\mathbf{F}_h$ can be obtained as follows:

$$\mathbf{T}_h = \sum_{k=1}^{M} \mathbf{r}^k \times \left[\rho_w C_f S^k \,|\, \mathbf{U}_{\parallel}^k \,|\, \mathbf{U}_{\parallel}^k - \left(\frac{1}{2} \rho_w C_d S^k \left[(\mathbf{U}^k \cdot \mathbf{n}^k) \right]^2 \mathbf{n}^k \right) \Big|_{(\mathbf{U}^k \cdot \mathbf{n}^k)<0} \right] \qquad (7)$$

where $\mathbf{r}^k$ is the radius vector directed from the body's centre of mass to the geometrical centre of the k-th triangle. As shown below, Eqs. (6) and (7) provide an effective way to parameterise the fluid drag on ice features, and allows the consideration of different ice shapes and various flow regimes, e.g., propeller jets. Further details on the inclusion of propeller flow within SAMS' hydrodynamic module are given in another paper within this special issue, Tsarau et al. (2018), which also presents the OATRC2015 experimental data to calibrate the presented model.

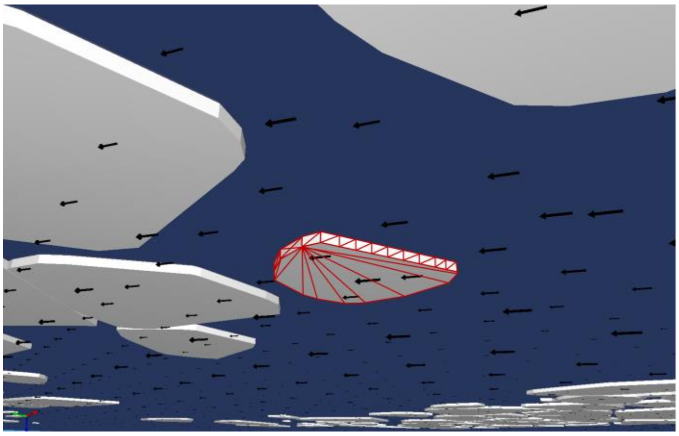

Fig. 13. Ice floes represented by triangular meshes. The mesh is automatically refined by SAMS if the flow is not uniform.

4.2 Validation of SAMS using OATRC2015 full-scale data

The different modules described above were developed over many years by a number of researchers at NTNU. Despite the common vision of creating a numerical simulator for floaters in ice, the development of each module was carried out almost independently from the other modules. At that stage, many attempts were also made to validate each module against available full-scale and lab-scale data (Lu et al., 2015a; Lu et al., 2015b; Lu et al., 2016c, Tsarau and Løset, 2015; Tsarau et al., 2014). In 2016, ArcISo was established to refactor and integrate the different modules to build SAMS as a versatile and highly accurate high-fidelity numerical simulator of offshore structures in floe-ice conditions. To achieve this, a firm quality control system was implemented to ensure clean, readable, maintainable code that is tested and verified. In addition, great attention is given to the validation and documentation of SAMS.

In regard to the validation of SAMS, the OATRC2015 expedition provides ample cases and data sets to validate each module separately and collectively. For example, within this special issue, Tsarau et al. (2018) utilised the OATRC2015 data to validate the developed propeller wash model within the hydrodynamic module, and Lu et al. (2018a; 2018b) developed and validated analytical formulas to account for the kinking behaviour of long splitting cracks, and these analytical formulae became a further enrichment to the existing fracture module. The following text, on the other hand, focus on the overall validation of SAMS using OATRC2015 full-scale data.

We present a case during Oden's transit in the Marginal Ice Zone (MIZ). On September 30th, 2015, after completing all the research activities, the fleet began the returning voyage. Oden began her return journey at 06:00:00. Approximately 6 hours before that, the helicopter on-board of Oden was on a mission to map the ice conditions in the MIZ ahead of Oden. The helicopter's flying route above ground is depicted in Fig. 14, together with sample images taken by the helicopter camera system illustrating the corresponding ice conditions. The purpose of the flight was to characterise the ice across the ice edge and partly along it. The flight headed south towards the ice edge, then turned west at the edge before returning up north to Oden.

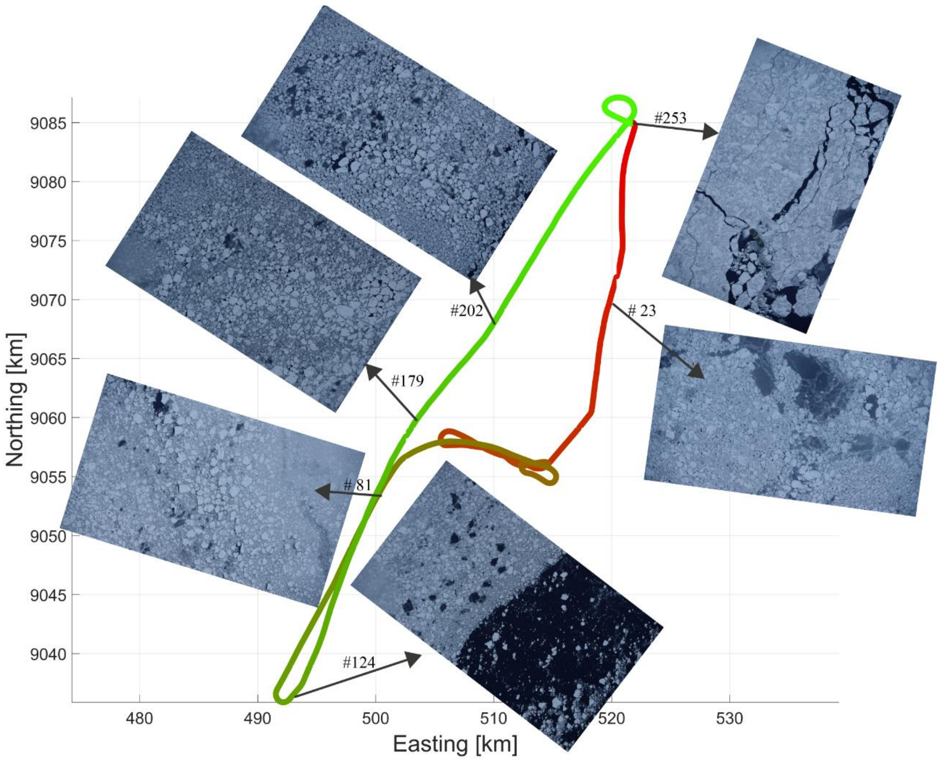

Fig. 14. Helicopter's flying route (starting from red and gradually changing into green) with sampled images of the ice conditions.

Oden was drifting at 0.5 m/s in the southwest direction from 00:00:05 September 30th until she began the transit on 06:00:00 September 30th. The track of Oden and the helicopter route above ground are illustrated in Fig. 15. In addition, if the sea-ice follows a similar drift path as Oden, we can also plot the estimated ‘helicopter’s flying route’ above the ice after considering the ice drift correction. We can see that for the time window from 06:49:00 till 07:05:00, there is a good overlap between Oden’s track and the filmed ice condition along the helicopter route.

Ideally, it is possible to utilise all the collected images (e.g., from Images #179 to #253 in Fig. 14) along the route to build a large mosaic image characterising the detailed ice conditions Oden has transited through. Such information can be utilised to initialise the ice condition in SAMS, and we can explicitly simulate the transiting process of Oden within the given ice field. The simulation output would be a time history of the resistance encountered by Oden. These simulated results can, in turn, be compared with the ice resistance calculated based on the on-board IMUs’ measurements (Kjerstad and Skjetne, 2016; Kjerstad and Lu, 2018). This gives us an opportunity to utilise the OATRC2015’s data to validate the capabilities of SAMS to model Oden’s transit in the MIZ.

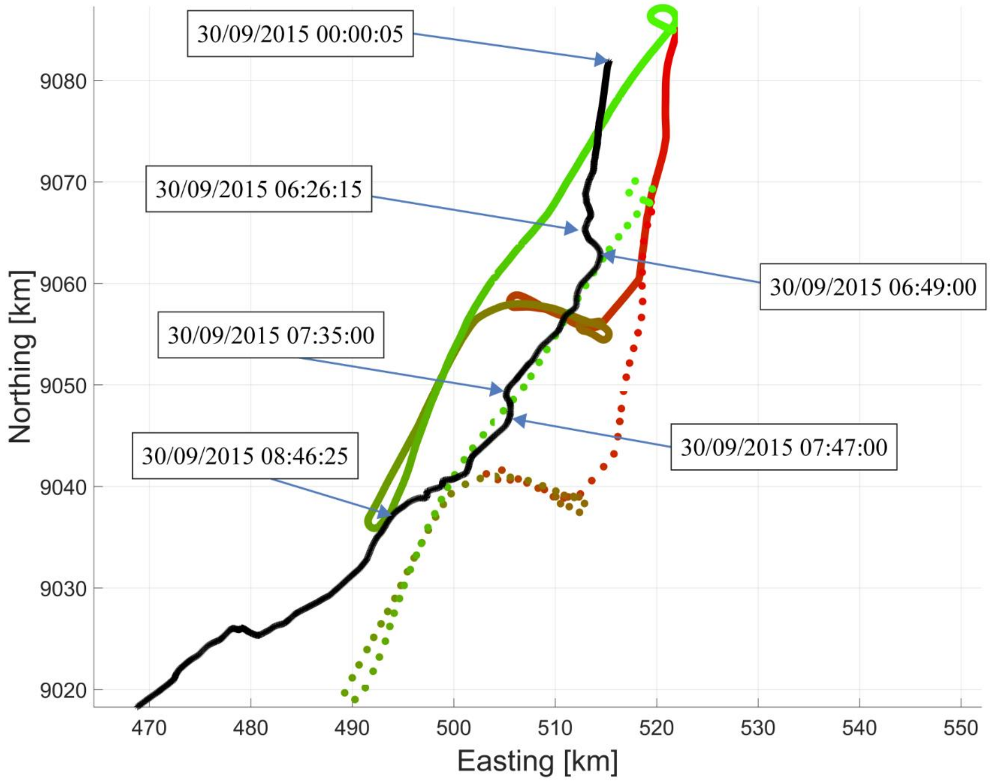

Fig. 15. Oden's transit track (in dart line from north to south); the in-advance helicopter's flying route (solid line in colour, from red to green); and the estimated flying route after ice drifting correction (dotted line in colour, from red to green).

4.3 A Validation Sample

In this paper, instead of attempting a full validation scenario along the entire transit route, we selected one representative image (i.e., #179) from which ice conditions (i.e., ice concentration, floe size distribution, and floe geometries) are extracted based on image processing techniques (Zhang and Skjetne, 2015). The digitalised ice field, after resolving the overlap between the digitised floes, is imported into SAMS for further simulation. Fig. 16 illustrates the original ice field Image #179, and its final digitalisation composed of discrete ice floes.

The geometrical model for a floater in SAMS is stored in the Wavefront OBJ format (.obj file), which can be generated by using 3D graphics software, and may comprise multiple triangle meshes. Each of the meshes is assumed to represent a convex hull. For the simulations presented in this paper, Oden’s geometry was accurately digitalised using readily available software packages, such as *Blender* and *FreeCAD*. The input model of Oden contained 35 convex bodies, which in total contained 2240 vertices, 6510 edges and 4338 faces. The large number of mesh elements allow a very detailed approximation of Oden’s hull, as seen in Fig. 17.

Furthermore, the input mechanical parameters of sea-ice in all the simulations presented in this paper are summarised in Table 2. Most of the values are chosen with reference to Timco and Weeks (2010), with a preference for engineering applications. For the fracture toughness of sea ice, the chosen value is based on the work of Dempsey et al. (1999). Note that the form drag coefficient is set to zero. As the thickness of the ice floes compared to their typical sizes is small, and no significant broken-ice accumulation was observed for the entire run, the form drag coefficient is set to zero, i.e., only the frictional component of the drag is simulated.

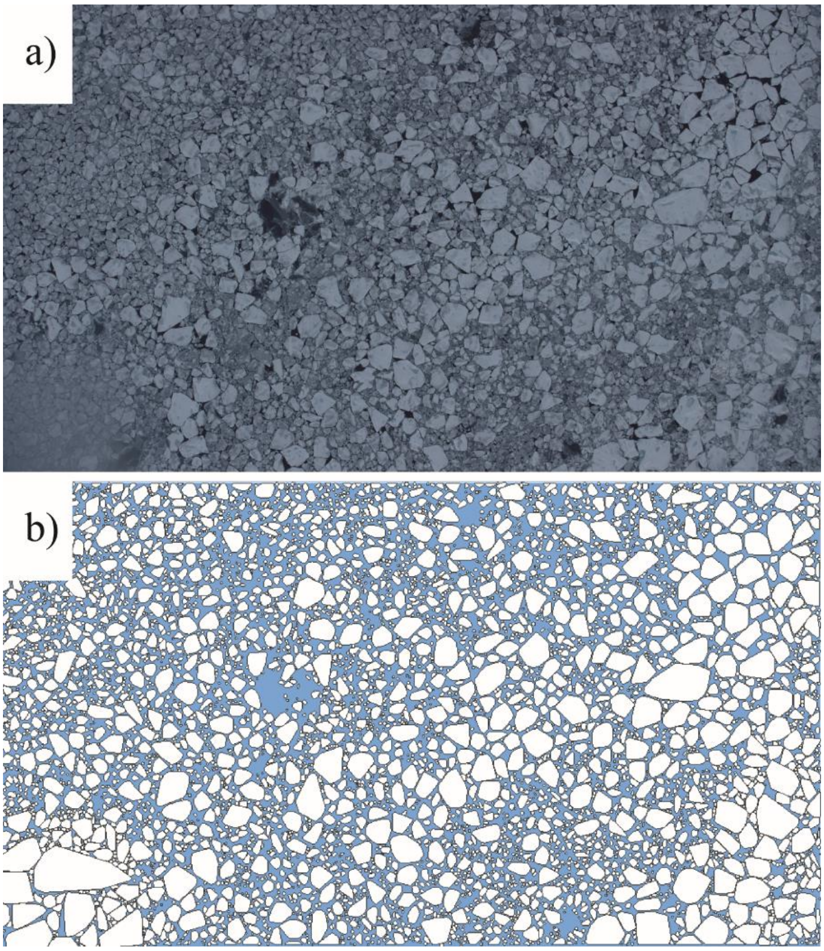

Fig. 16. a) Initial helicopter camera image; and b) Digitalised ice field for simulation input.

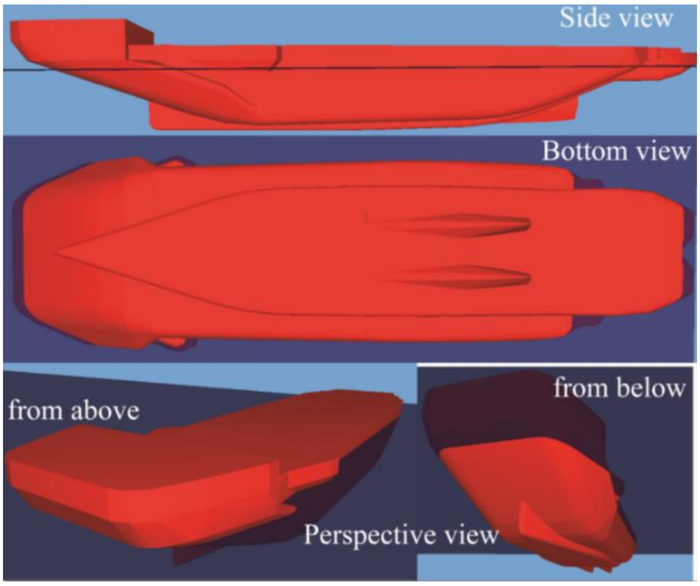

Fig. 17. Geometric representation of Oden.

Table 2. Inputs for the simulations.

$\Delta t = 0.1\text{s}$	Simulation time step;
$\rho_i = 900\,\text{kg/m}^3$	Ice density;
$\rho_w = 1025\,\text{kg/m}^3$	Water density;
$C_f = 0.005\ [-]$	Skin friction coefficient;
$C_d = 0.000\ [-]$	Form drag coefficient;
$h = 1\text{m}$	Ice thickness;
$E = 5\,\text{GPa}$	Young’s modulus;
$v = 0.3\ [-]$	Poisson ratio;
$K_{IC} = 150\,\text{kPa}\sqrt{\text{m}}$	Fracture toughness;
$\sigma_c = 2\,\text{MPa}$	Compressive strength;
$\sigma_f = 500\,\text{kPa}$	Flexural strength;
$\mu_{ii} = \mu_{is} = \mu_{iw} = 0.1\ [-]$	Ice-ice, ice-structure, and ice-boundary friction coefficient.

4.3.1 <u>Simulation of the Oden transit in the MIZ by SAMS</u>

At first, we use the representative ice field in Fig. 16 for Oden's transit simulation. A visual illustration of the simulated transit is illustrated in Fig. 18. Given the almost linear motion of Oden illustrated in Fig. 15, the simulation was performed with only one degree of freedom (1 DoF), i.e., with a constant speed of 6 m/s in the surge direction. The simulated ice load history in the surge direction F_{sim} together with its averaged ice resistance, $\bar{F}_{sim} = 851\,\mathrm{kN}$, are shown in Fig. 19. These simulated results shall be compared with ice load estimated from the field measurements.

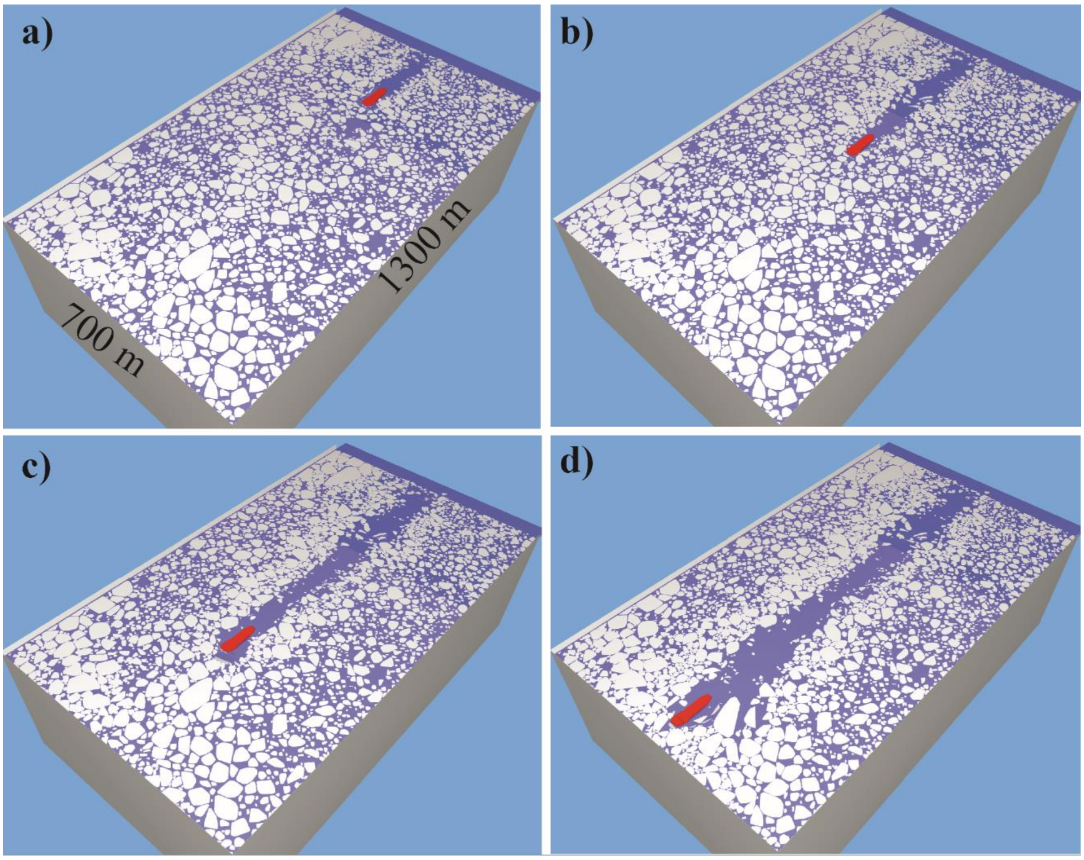

Fig. 18. Visualisation of the simulated ship transit directly in the ice field captured in Fig. 16.

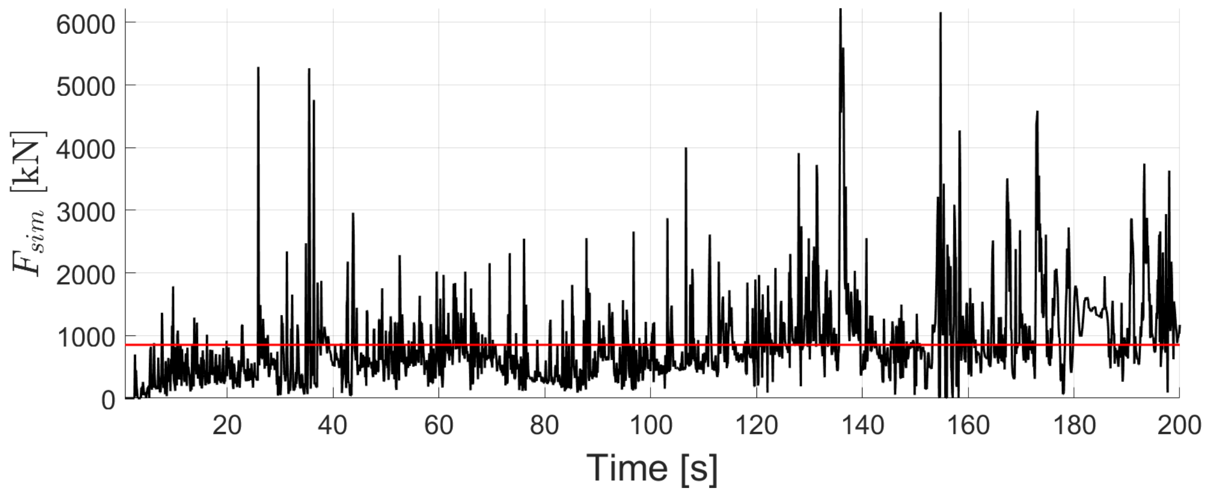

Fig. 19. Simulated ice load history (in black) in the surge direction (unfiltered) and its averaged ice resistance (in red solid line).

4.3.2 Extended simulation of the Oden transit in the MIZ by SAMS

We see from the simulation in Fig. 18 that the majority of ice floes in the width direction are not mobilised during the simulation. Moreover, the simulated transit distance is relatively short to demonstrate SAMS' capacity to efficiently perform large scale simulations. Therefore, in this section, we extend the ice field based on ice information extracted from Fig. 16. Given the identified ice floe geometry, we can characterise each ice floe's size with the Mean Clipper Diameter (MCD), as shown in Eq. (8).

$$\mathrm{MCD} = 2\left(\frac{\text{Floe Area}}{\pi}\right)^{1/2} \tag{8}$$

The floe size distribution for the ice field shown in Fig. 16 is fitted by three proposed distribution functions (Lu et al., 2008) and is presented in Fig. 20. Among these three distributions, we see that the truncated Weibull distribution gives the best fitting to the helicopter image data. The truncated Weibull distribution's formulation together with the fitted parameters are presented in Eq. (9).

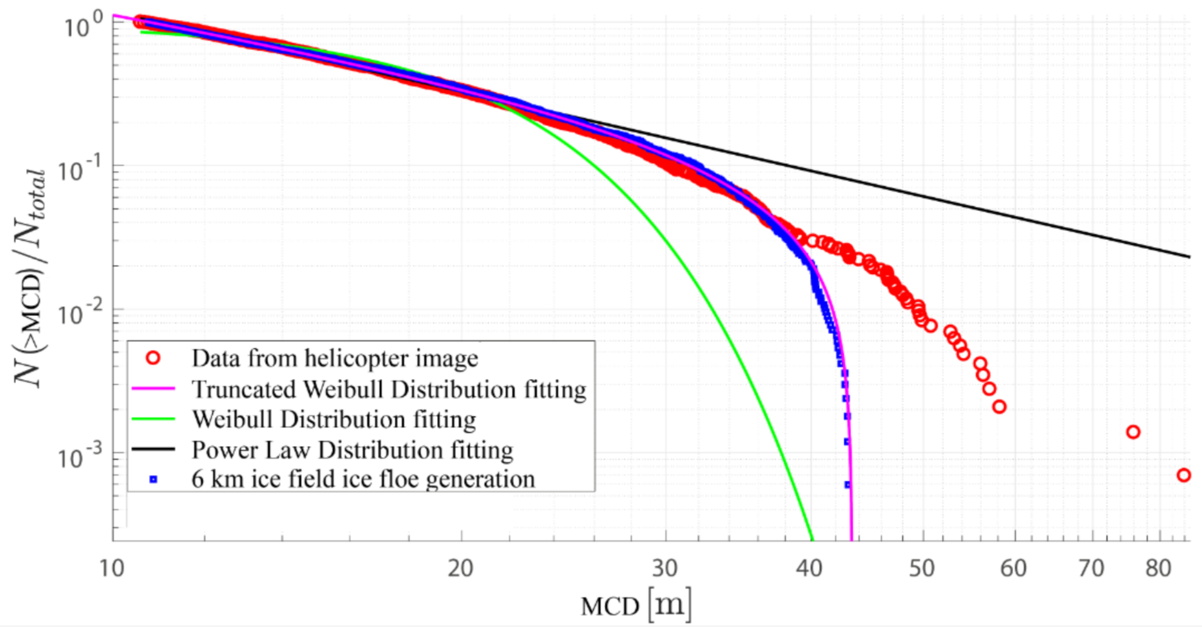

Fig. 20. Fitting floe size data from Fig. 16 with three different distribution functions and generating ice floes filling a 6 km long ice field.

$$\frac{N(>\mathrm{MCD})}{N_{total}} = C_0(\mathrm{MCD}^{-D} - L_r{}^{-D}) = 27.25(\mathrm{MCD}^{-1.32} - 43.41^{-1.32}) \quad (9)$$

where N_{total} is the total number of the generated ice floes.

Using the truncated Weibull distribution above, we generated an ice field that is 150 m wide and 6 km long. The 150-m width leaves a space which is about twice the ship's beam width. Based on previous simulation experiences, and the transit simulation results shown in Fig. 18, this leaves a reasonable margin between the structure and the wall, with negligible boundary effects. The visual illustration of the extended simulation is presented in Fig. 21 with: a) an overview at different simulation times; b) and c) nearby interaction zones near the ship bow and the wake region.

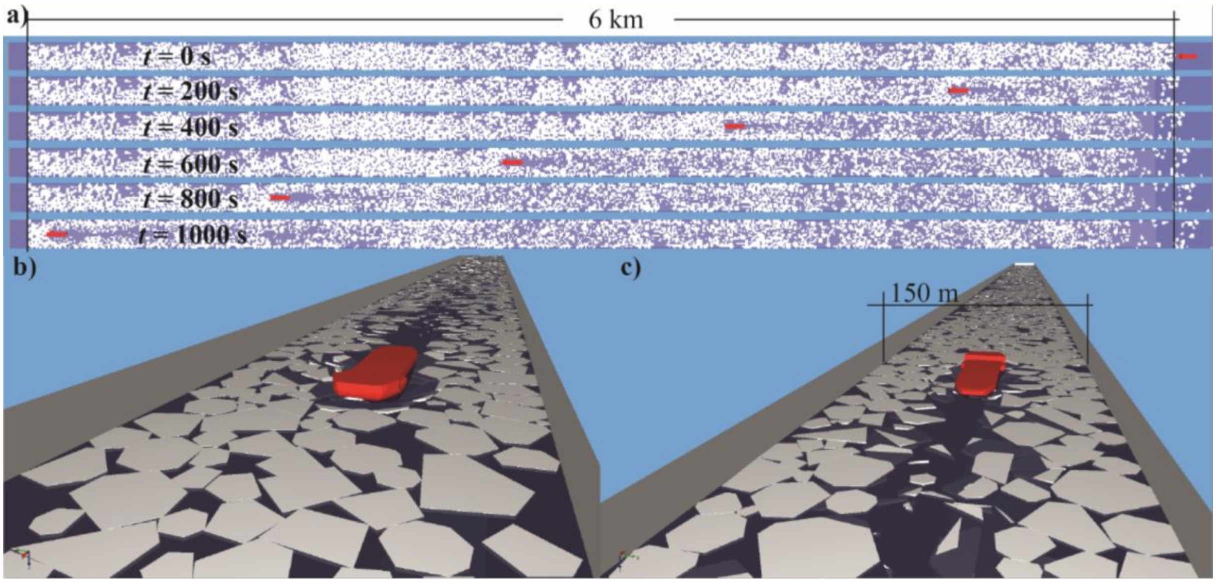

Fig. 21. Visualisation of the simulated ship transit in a 6-km ice field extended from Fig. 16.

Similarly, the simulated ice load time history F_{sim} and its averaged ice resistance $\bar{F}_{sim} = 1006\,\mathrm{kN}$ are illustrated in Fig. 22. These simulated results shall be compared with the ice load estimated through the field measurements.

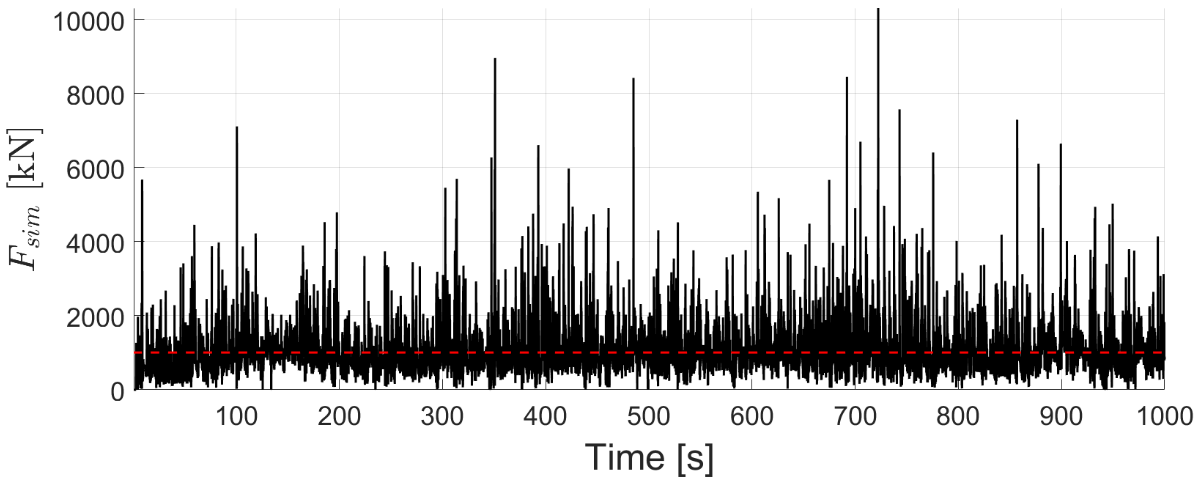

Fig. 22. Simulated ice load history (black) from an extended ice field in the surge direction (unfiltered) and its averaged ice resistance (red dashed line).

4.3.3 Full-scale ice load identification/calculation

To verify the simulation results in the previous sections, it is necessary for us to obtain the ice load history encountered by Oden during the transit. However, direct measurement of global ice load acting on an icebreaker is rather challenging, if it is at all possible. Instead, we shall utilise several indirect measurements to back-calculate the global ice load history. These measurements include: 1) four Inertia Motion Units (IMUs) to obtain the ship's acceleration history $\dot{v}$; 2) the ship's propulsion data; and 3) ship data (including the ship's position and heading, wind direction and speed, and geometry of the ship). The identification model follows the formulations by Fossen (2011) and is written in Eq. (10).

$$M\dot{v} = \tau_a + \tau_h + \tau_w + \tau_i \tag{10}$$

in which,

M is Oden's mass matrix in the surge heave and yaw directions; and it is estimated in accordance with Table 1, i.e., $M = \mathrm{diag}[m, m, 0.7m/12 \cdot (L_{ship}^2 + B_{ship}^2)] = 10^6\,\mathrm{diag}[13\,\mathrm{kg}, 13\,\mathrm{kg}, 9286.4\,\mathrm{kg}\cdot\mathrm{m}^2]$;

$\dot{v}$ is Oden's accelerations in the surge heave and yaw directions measured by the IMUs.

τ_a, τ_h, τ_w, and τ_i are ship propulsion, hydrodynamic resistance, wind resistance and global ice load respectively. Their detailed formulation and calculations are presented in the companion paper (Kjerstad and Lu, 2018). In this paper, the results of the ice load identifications/calculations are presented in Fig. 23. Note the positive ice load at the start of the time series in the surge direction. This is due to the sensitivity of the identification model to the initial conditions.

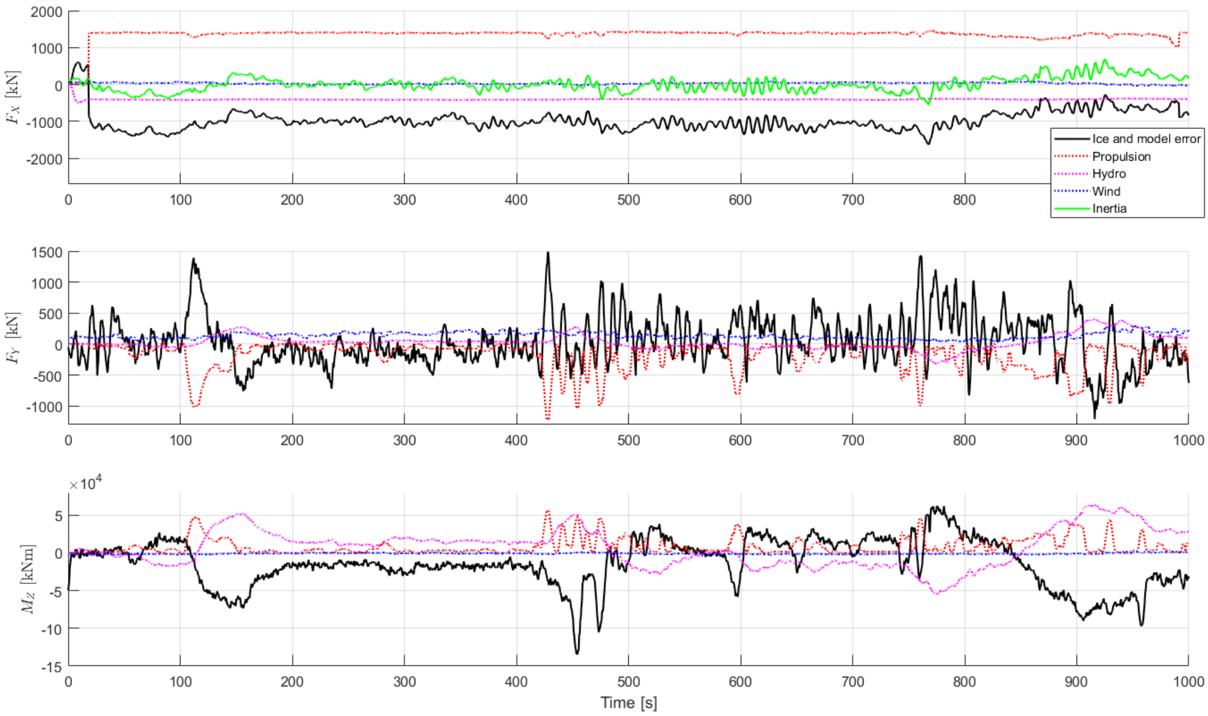

Fig. 23. Different load components' history during Oden's transit within the selected time window.

4.3.4 <u>Comparison between simulation results and measurement-based calculations</u>

Fig. 24 compares the simulation results with the ice loads back-calculated from the full-scale measurements. The raw simulation results are shown in Fig. 22, while those in Fig. 24 are smoothed using a moving average over a window of 10 s.

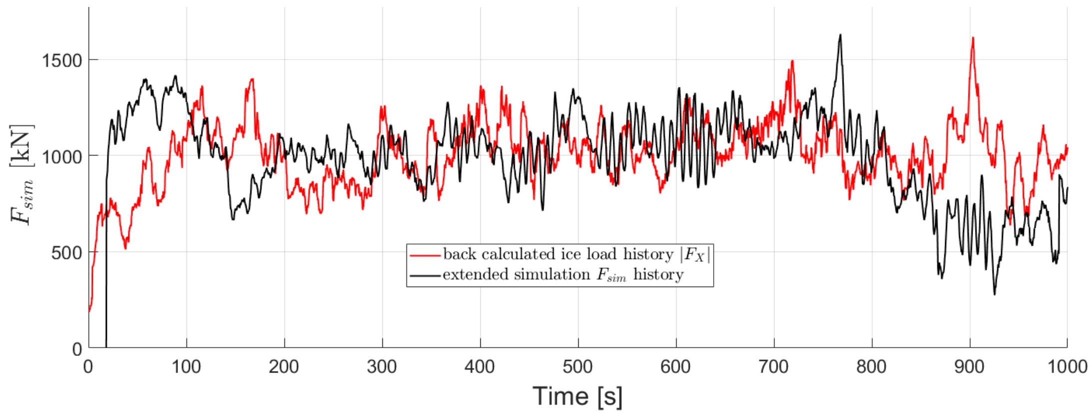

Fig. 24. Time history comparison between back calculated ice load and by extended simulation.

Even when the ice field for the short simulation (200 s) is digitised directly from the available image, it is highly unlikely that Oden transited through the exact same ice field (i.e., the initial conditions change due to wind and currents). For the extended simulation (1000 s), the ice field is generated based on a statistical distribution. All this suggests that we can compare the simulation results and the measurements only in a statistical sense. The statistical parameters, e.g., the mean, of both the simulations and the measurements are shown in Fig. 25. The comparison shows a favourable agreement between the simulation results and the full-scale data and, especially, as is to be expected, for the extended simulations.

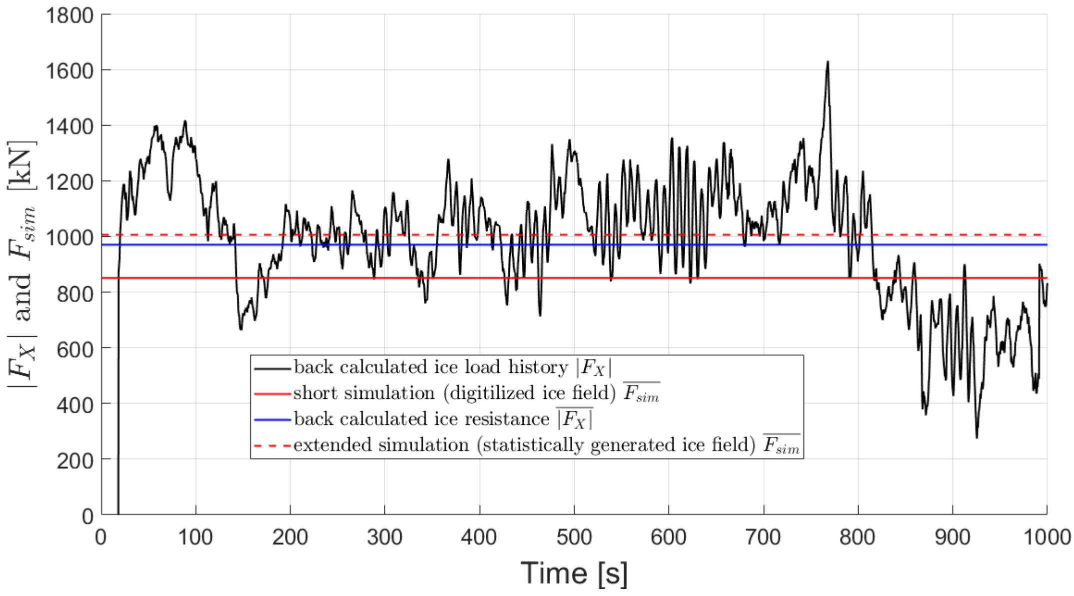

Fig. 25. Comparison between simulation and back calculations based on measurements.

4.3.5 <u>Discussion of the validation sample</u>

Fig. 25 presents a comparison between the simulation results and the ice loads back-calculated from the full-scale measurements. Even though several simplifications were made in the simulation set-up, the averaged ice resistance from the simulations appears to be rather consistent. As will be discussed in detail in the following text, these simplifications are reasonable given the current ship transit scenario. In this validation task, we utilised a representative ice field and conducted a direct simulation. Furthermore, we generated an extended ice field from this representative ice field, and an extended simulation was conducted. Although the ice field is not exactly the ice field Oden has transited through, from a statistical sense, the averaged ice resistance from both the simulation and measurement are not expected to differ greatly. This is presented in Fig. 25, signifying the high fidelity of the simulations that were conducted.

In addition, Fig. 24 takes a further step, and compares the ice load histories from the simulations and the measurements. The simulated time history was smoothed by a moving average with a 10-s time window before it was overlaid upon the measurement-based time history. The chosen 10-s time window is in accordance with the criteria adopted when processing the full-scale measurements to back calculate the ice load, i.e., down sampling all the measured data and filtering the high frequency part of the measurement (Kjerstad and Lu. 2018). After some trial and errors, the 10-s time window gives a visually comparable variation frequency against the measurement-based ice load history. However, the magnitude of variation from the measurement-based ice load history is much smaller than the raw data that was simulated in Fig. 22. For one reason, this is because of the back-calculated data is, by itself, down sampled and filtered along the processing procedures (Kjerstad and Lu, 2018). For another reason, this is attributed to our simplification of a displacement controlled simulation, i.e., Oden was travelling with a constant speed of 6 m/s in the surge direction in the simulation, whereas in reality, the surge acceleration varies continuously throughout the transit. Therefore, the magnitude of the simulated ice load can easily builds up while encountering difficult ice features, whereas in reality, the free floating structure can give away in form of, e.g., deceleration, and thereby milden the ice load. An improvement to this would be to feed Oden with the available propulsion during the simulation and let the behaviour of the structure (i.e., transit speed and displacement) and the overall ice resistance depend entirely on the ice condition that is encountered. Thereafter, it is expected that we can achieve a better comparison in the ice load history's variations in terms of both its frequency and magnitude.

- A sample validation instead of full simulation

In this validation sample, the entire ship transit over 20 km from 06:49:00 to 07:35:00 was not simulated. Instead, we only digitalised one ice field image covering 1.3 km by 700 m. Given the ice field images taken from the helicopter illustrated in Fig. 14 together with the ship route above the ice shown in Fig. 15, we believe the selected ice field is general enough to yield comparable ice resistance data. Therefore, for both the short and extended simulation, all the ice information used was derived from this representative image. Generally, we can see that a rather favourable comparison is achieved in Fig. 255, signifying the simulation capability of SAMS in terms of ship transit in a broken ice field.

- 1-DoF simulation

For the conducted simulation, another point worth mentioning is that only a 1-DoF simulation was conducted for simplicity and practical reasons. This is reasonable considering Oden's velocity in the surge, sway and heave direction during the transit (see Fig. 26). A dominant velocity in the surge direction can be found in Fig. 26. Comparatively, less motion is detected in the sway and heave direction. Particularly, the heave is so small such that its negligence in Eq. (10) is justified.

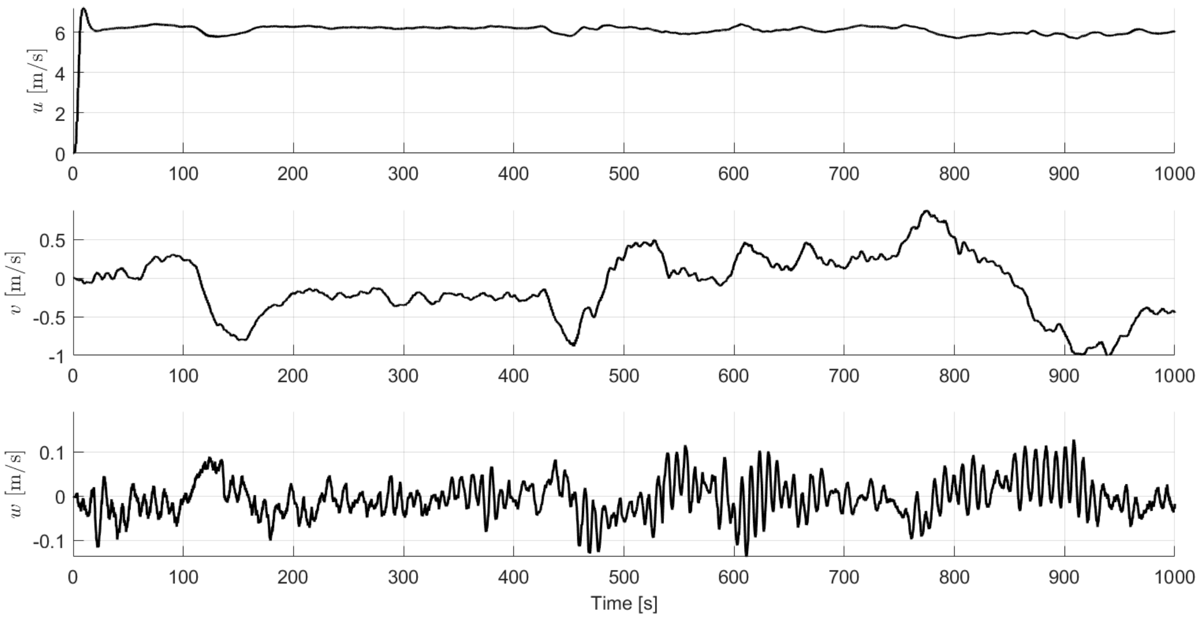

Fig. 26. The velocities in surge u, sway v and heave w during Oden's transit.

- Simulation features

Aside from the global ice resistance's simulation, it is also important to stress the detailed physical processes that SAMS has captured during the simulation. Fig. 27a and b illustrate SAMS' multi-body dynamics' capability to capture the 6 DoFs motion of an ice floe. In the consecutive image of Fig. 27c, the ice floe's splitting fracture is demonstrated. Most ice floes that interacted with Oden within the simulated ice field (i.e., Fig. 18 and Fig. 21) are relatively small ice floes, with $\mathrm{MCD} \leq 40\,\mathrm{m}$. According to previous studies, local bending failure is less likely to occur. This is in accordance with the current simulations.

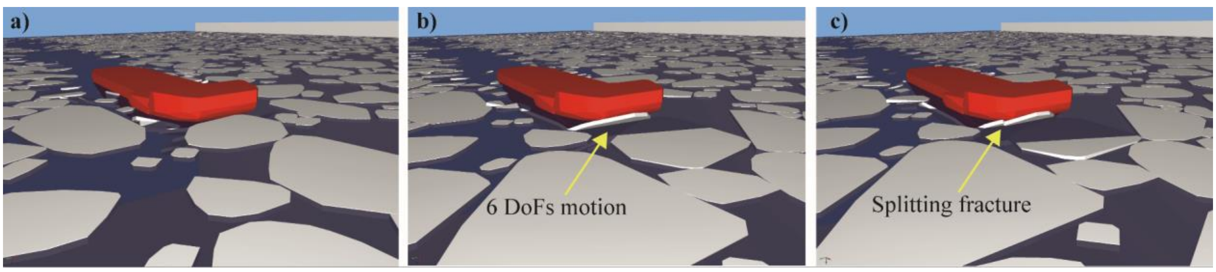

Fig. 27. Detailed physical processes simulated within SAMS.

In addition to the multi-body interactions and the ice floe's failure mode demonstrations, a different scenario with a constant 0.5 m/s current flowing with 45° to Oden's surge direction is simulated with SAMS and is illustrated in

Fig. 28. With the presence of current drag, ice floes within the ice field are packing to the upper right corner of the simulation domain. This visually demonstrated the effectiveness of the hydrodynamic module within SAMS.

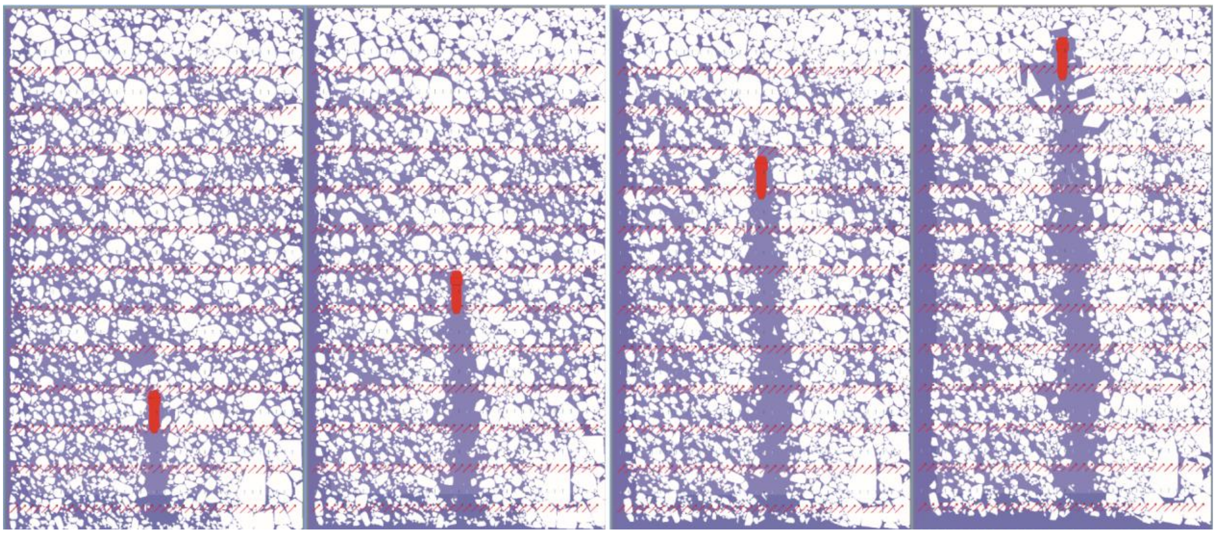

Fig. 28. Illustration of the hydrodynamic module introducing the influence of current force (0.5 m/s and with 45 deg. with reference to the surge direction) in the entire simulated ice field.

5 Conclusions

OATRC2015 is a good example for the cooperation between academia, industry and governmental research sectors. The scientific scope of OATRC2015 included three major fields of studies, namely: 1) collection of full-scale data necessary to build, calibrate and validate numerical models for floaters in ice, 2) collection of full-scale data necessary to build, calibrate and validate numerical models for Ice Management operations, and 3) collection of data for health, safety and environmental research. Safety and the environment were considered seriously in the different phases of the project, and OATRC2015 ended without a single accident. In summary, OATRC2015 succeeded in the overall cruise objective “to perform a safe cruise collecting valuable and important scientific data and to perform full-scale field trials for testing of key technologies.” During the 14-day field programme, many research activities were carried out and the research cruise produced a considerable amount of valuable data in the following areas:

- Monitoring of ice conditions using different camera systems
- Characterisation of ice using helicopter and vessel observations
- Monitoring of ice with satellite data

- Collection of marine radar data
- Collection of ice drift data using beacons
- Study of ice management tactics using the Oden and Frej
- Collection of local ice loads data on the Frej
- Collection of ship motion measurements using Inertial Measurement Units (IMU)
- Collection of vessel performance data
- Measurement of ice thickness with EM and shipborne radar
- Study of brash ice
- Testing of high-speed Arctic communications
- Investigations of vibrations on the icebreaker crew
- Water sampling and biodiversity
- Collection of marine mammal observations

The data and results from the programme will continue to be used to promote safe and sustainable maritime operations in the Arctic. In the second part of this paper, we used Oden's transit data (from 06:49:00 to 07:05:00 on September 30th) to validate the simulator for Arctic Marine Structures (SAMS). In the validation task, one representative ice field image taken by the helicopter along Oden's transit route was chosen to digitalise the ice field to extract information, such as ice floe size, geometry and locations. Given such real field ice information, we reconstructed this ice field (1.6 km by 0.7 km) within SAMS, and directly simulated Oden's transit within it. Furthermore, we further extended this ice field into a much longer ice field (i.e., 6 km by 150 m) by generating ice floes, whose sizes follow a truncated Weibull distribution. Thereafter, a much longer simulation (1000 s) is simulated within this extended ice field.

- Statistically, SAMS yields rather satisfactory ice resistance values for both the short and extended simulations, which have -13.1% and 2.7% errors compared to the value calculated based on measurements;
- Through the validation process, different modulus within SAMS are collectively verified. Individually, the functionalities of different modulus are visually demonstrated. This includes: the multi-body dynamics accounting for each individual ice floe's motion and their interactions with themselves and the structure; the multi-failure modes of each ice floe according to previous theoretical development; and the hydrodynamic module's capability to consider the effect from the ambient fluid (both air and water).

Acknowledgements

The Oden Arctic Technology Research Cruise 2015 (OATRC2015) was supported by the ExxonMobil Upstream Research Company and was performed by the Norwegian University of Science and Technology (NTNU) in cooperation with the Swedish Polar Research Secretariat (SPRS) and the Swedish Maritime Administration (SMA). OARTC2015 was successful due to the contributions from many individuals from the organisations listed in Table 3. Special thanks are given to the crews of the icebreakers, Oden and Frej.

Table 3. Alphabetical listing of participating organisations

Avron Ritch Consulting Ltd.	ExxonMobil Upstream Research Company	Red Rental
Canatec Associates International Ltd.	Kallax Flyg	Swedish Maritime Administration
C-Core	Lulea University of Technology	Swedish Polar Research Secretariat
Chalmers University of Technology	Nordic Unmanned	Trumbull Unmanned
Dansk Bioconsult - Marine Observers	Norwegian University of Science and Technology	University Centre in Svalbard
European Helicopter CenterCentre	Oceaneering	University of Gothenburg

We acknowledge the use of Rapid Response imagery from the Land, Atmosphere Near real-time Capability for EOS (LANCE) system, operated by the NASA/GSFC/Earth Science Data and Information System (ESDIS) with funding provided by NASA/HQ.

References

Alawneh, S., Dragt, R., Peters, D., Daley, C. and Bruneau, S., 2015. Hyper-Real-Time Ice Simulation and Modeling Using GPGPU. IEEE Transactions on Computers, 64(12): 3475-3487.

Baird, D. J. and Hajibabaei, M., 2012. Biomonitoring 2.0: a new paradigm in ecosystem assessment made possible by next-generation DNA sequencing. Molecular Ecology, 21: 2039–2044. doi:10.1111/j.1365-294X.2012.05519.x.

Dempsey, J.P., Adamson, R.M. and Mulmule, S.V., 1999. Scale effects on the in-situ tensile strength and fracture of ice. Part II: First-year sea ice at Resolute, NWT. International journal of fracture, 95(1): 347-366.

Dempsey, J.P. and Mu, Z., 2014. Weight function for an edge-cracked rectangular plate. Engineering Fracture Mechanics, 132(0): 93-103.

Dudal, A., Septseault, C., Beal, P.-A., Le Yaouanq, S. and Roberts, B., 2015. A New Arctic Platform Design Tool For Simulating Ice - Structure Interaction, The 23rd International Conference on Port and Ocean Engineering under Arctic Conditions, Trondheim, Norway.

Fenz, D., Younan, A., Piercey, G., Barrett, J., Ralph, F., and Jordaan, I., 2018. Field Measurement of the Reduction in Local Pressure from Ice Management. Cold Regions Science and Technology (Submitted to this special issue)

Fossen, T.I., 2011. Kinematics, Handbook of Marine Craft Hydrodynamics and Motion Control. John Wiley & Sons, Ltd, pp. 15-44.

Haas, C., Le Goff, H., Audrian, S., Perovich, D., Haapala, J., 2011. Comparison of seasonal sea-ice thickness change in the Transpolar Drift observed by local ice mass-balance observations and floe-scale EM surveys. Annals of Glaciology, Vol. 52, Issue 57 Part 1, pp. 97-102.

Holub et al. (2017) Holub, C., Matskevitch, D., Kokkinis, T., and Shafrova, S., 2018. Near-Field Ice Management Tactics-Simulation and Field Testing. Cold Regions Science and Technology (Submitted to this special issue)

Hamilton, J., Kokkinis T., Holub C., Matskevitch D., Cheng T., Harris M., and Shafrova S., 2016. Near-Field Ice Management Tactics for Floating Drilling in Arctic Pack Ice. In Proc. of the Arctic Technology Conference (ATC), St. John's, Newfoundland and Labrador, Canada, October 24-26, 2016. OTC-27341.

Heyn, H. M., Skjetne R., 2016. A system for measuring ice-induced accelerations and identifying ice actions on the CCGS Amundsen and a Swedish ATLE-class icebreaker. In Proc. of the 35th ASME International Conference on Ocean, Offshore and Arctic Engineering (OMAE), June 19-24, 2016, Busan, Korea.

Heyn, H.M., and Skjetne, R., 2018. A time-frequency analysis technique for acceleration data from ship-ice interaction events. Cold Regions Science and Technology (Submitted to this special issue)

Johannesson, O., 2016. Investigation of exposure to whole body vibration for icebreaker crew - An investigation of whole body vibration exposure during ice-breaking in Arctic sea as a part in the "Oden Arctic Technology Research Cruise" 2015, Swedish Maritime Administration, 35 pp.

Kim, E. and Gagnon, R.E., 2016. A preliminary analysis of the crushing specific energy of iceberg ice under rapid compressive loading.

Kinnunen, A., Tikanmäki, M. and Heinonen, J., 2016. An energy model for ice crushing in ice-structure impact, 23 r d IAHR International Symposium on Ice, Ann Arbor, Michigan, USA, pp. 1–8.

Konno, A. and Mizuki, T., 2006. Numerical Simulation of Pre-Sawn Ice Test of Model Icebreaker Using Physically based Modelling, Proceedings oh the 18th IAHR International Symposium on Ice, Sapporo, Japan, pp. 17-23.

Lu, P., Li, Z.J., Zhang, Z.H. and Dong, X.L., 2008. Aerial observations of floe size distribution in the marginal ice zone of summer Prydz Bay. Journal of Geophysical Research: Oceans, 113(C2): n/a-n/a.

Lu, W., Lubbad, R. and Løset, S., 2015a. In-plane fracture of an ice floe: A theoretical study on the splitting failure mode. Cold Regions Science and Technology, 110(0): 77-101.

Lu, W., Lubbad, R. and Løset, S., 2015b. Out-of-plane failure of an ice floe: Radial-crack-initiation-controlled fracture. Cold Regions Science and Technology, 119: 183-203.

Lu, W., Zhang, Q., Lubbad, Løset, S., R., Skjetne, R., 2016a. A Shipborne Measurement System to Acquire Sea Ice Thickness and Concentration at Engineering Scale. In Proc. of the Arctic Technology Conference (ATC), St. John's, Newfoundland and Labrador, Canada, October 24-26, 2016. OTC- 27361.

Lu, W., Lubbad, R., Løset, S., Skjetne, R., 2016b. Parallel Channel Tests during Ice Management Operations in the Arctic Ocean. In Proc. of the Arctic Technology Conference (ATC), St. John's, Newfoundland and Labrador, Canada, October 24-26, 2016. OTC- 27344.

Lu, W., Lubbad, R., Løset, S. and Kashafutdinov, M., 2016c. Fracture of an ice floe: Local out-of-plane flexural failures versus global in-plane splitting failure. Cold Regions Science and Technology, 123: 1-13.

Lu, W., Lubbad, R., Shestov, A., and Løset, S., 2018a. Parallel Channels' Fracturing Mechanism during Ice Management Operations. Part I: Theory. Cold Regions Science and Technology (Submitted to this special issue)

Lu, W., Lubbad, R., and Løset, S., 2018b. Parallel Channels' Fracturing Mechanism during Ice Management Operations. Part II: Experiment. Cold Regions Science and Technology (Submitted to this special issue)

Lubbad, R. and Løset, S., 2011. A numerical model for real-time simulation of ship-ice interaction. Cold Regions Science and Technology, 65(2): 111-127.

Matskevitch, D., Løset, S., Shafrova, S., Mitchell, D., and Holub, C., 2016. Application of Satellite Remote Sensing Data during OARTC 2015 Research Expedition. In Proc. of the Arctic Technology Conference (ATC), St. John's, Newfoundland and Labrador, Canada, October 24-26, 2016. OTC-27339.

Metrikin, I., 2014. A software framework for simulating stationkeeping of a vessel in discontinuous ice. Modeling, Identification and Control, 35(4): 211.

Mitchell, D. A., and Shafrova, S., 2018. Application of a Free Drift Tactical Ice Forecast Model in Pack Ice Conditions. Cold Regions Science and Technology (Submitted to this special issue)

N'Guessan, L., Springer, N., Borisenko, A., Singer, G., Shokralla, S., Hajibabaei, M., 2012. Next-Generation DNA-Based Approaches for Comprehensive Assessment of Marine Communities. SPE/APPEA International Conference on Health, Safety, and Environment in Oil and Gas Exploration and Production. Perth, Australia, September 11-13, 2012, SPE-157460, 13 p.

Piercy, G., Barrett, J., MacNeill, A., Ralph, F., Jordaan, I., Fenz, D.M., and Younan, A.H., 2016. Design of a Shipboard Local Load Measurement System to Collect Managed Ice Loads. In Proc. of the Arctic Technology Conference (ATC), St. John's, Newfoundland and Labrador, Canada, October 24-26, 2016. OTC-27342.

Shafrova, S., Holub, C., Harris, M., Cheng, T., Matskevitch, D., and Mitchell, D., 2016. Common Operational Picture COP Requirements for Floating Drilling in Pack Ice. In Proc. of the Arctic Technology Conference (ATC), St. John's, Newfoundland and Labrador, Canada, October 24-26, 2016. OTC-27343.

Timco, G.W. and Weeks, W.F., 2010. A review of the engineering properties of sea ice. Cold Regions Science and Technology, 60(2): 107-129.

Tsarau, A., Lubbad, R. and Løset, S., 2014. A numerical model for simulation of the hydrodynamic interactions between a marine floater and fragmented sea ice. Cold Regions Science and Technology, 103(Supplement C): 1-14.

Tsarau, A. and Løset, S., 2015. Modelling the hydrodynamic effects associated with station-keeping in broken ice. Cold Regions Science and Technology, 118(Supplement C): 76-90.

Tsarau, A., 2016. Hydrodynamic forces on ice floes in the propeller wash of a ship − full-scale experimental study. In Proc. of the 23rd International Symposium on Ice (IAHR), 31 May - 03 June 2016, Ann Arbor, Michigan, USA.

Tsarau, A., Lubbad, R., Løset, S., 2018. A numerical model for simulating the effect of propeller flow in ice management. Cold Regions Science and Technology (Submitted to this special issue)

Kjerstad, Ø.K., and Skjetne, R., 2016. Disturbance Rejection by Acceleration Feedforward for Marine Surface Vessels. Access IEEE, vol. 4, pp. 2656 – 2669.

Kjerstad, Ø.K. and Lu, W., 2018. A Method for Real-time Estimation of Full-scale Global Ice Loads on Floating Structures. Cold Regions Science and Technology (Submitted to this special issue)

Van den Berg, M., Lubbad, R., and Løset, S., 2017. An Implicit Time Stepping Scheme and an Improved Contact Model for Ice-Structure Interaction Simulations. Cold Regions Science and Technology (Submitted)

Yulmetov, R., Lubbad, R. and Løset, S., 2016. Planar multi-body model of iceberg free drift and towing in broken ice. Cold Regions Science and Technology, 121: 154-166.

Zhang, Q. and Skjetne, R., 2015. Image processing for identification of sea-ice floes and the floe size distributions. IEEE Transactions on Geoscience and Remote Sensing, 53(5): 2913-2924